Optimally sparse and adaptive far-field sampling and pattern reconstruction

Approach for faster calibration of antenna systems using compressed sensing

Master thesis: Electrical Engineering

Surya Natarajan Subramani

Optimally sparse and adaptive far-field sampling and pattern reconstruction

Approach for faster calibration of antenna systems using compressed sensing

by

Surya Natarajan Subramani

Student Name	Student Number
S.N.Subramani	5382629

Thesis supervisor:	Dr. Y.Aslan
Thesis Co-supervisor:	Dr. N.J.Myers
Thesis advisor:	Prof. DSc. A.Yarovoy
Project Duration:	December, 2022 - August, 2023
Faculty:	Faculty of Electrical Engineering, Mathematics and Computer Science, Delft

Cover:	ESA's Hertz Hybrid European RF and Antenna Test Zone for antenna testing (courtesy: ESA-Anneke Le Floc'h) (Modified)
Style:	TU Delft Report Style, with modifications by Daan Zwaneveld

TU Delft

Acknowledgements

I would like to use this part of my master's thesis to express my gratitude to the people without whom I would not have made it this far in both my academic as well as personal life.

First of all, I would like to express my deepest gratitude to Dr. Yanki Aslan, my daily supervisor, for his unwavering guidance, constant encouragement, and insightful feedback on my thesis, throughout the duration of this research. His expertise, dedication, and patience have been instrumental in shaping the direction of my work. I learned a lot from your academic strengths as well as work ethic.

I am also immensely thankful to Dr. Nitin Myers, my co-supervisor, for his valuable input and critical insights on compressed sensing that have significantly enhanced the quality of this thesis. His meticulous attention to detail and thoughtful suggestions have been invaluable.

I extend my heartfelt appreciation to Prof. DSc. Alexander Yarovoy, my thesis Advisor and Chairman of the MS3 group, for providing me with the opportunity to be a part of the group and for imparting knowledge and curiosity in my mind through his very interesting lectures throughout my masters study.

I would also like to express my gratitude to all the members at MS3 for their support and camaraderie. Their diverse perspectives have contributed to my growth as a researcher.

I am infinitely indebted to my parents for supporting and caring me in every possible way for me to try to achieve my dreams and ambitions. I love you both.

Finally, I would like to thank my friends at Delft and India. Your roasts, pranks, company, words and pat on the back kept me going at countless instances.

Thank you everyone.

Surya Natarajan Subramani
Delft, August 2023

Summary

Radiation pattern measurements is a critical step in characterizing antennas before they are used in any system for a specific application. To identify any defects or to acquire the true radiation characteristics of the antenna under test, densely sampled measurements are desired. However, this results in a time and cost expensive measurement process. Compressed sensing allows accurate reconstruction of radiation patterns using a reduced number of measurements. To ensure exact recovery, it is necessary to select an optimal sampling strategy as well as an effective reconstruction method.

In this thesis, the discrete Fourier transform (DFT) and spherical harmonic expansion of the electric field are used to obtain a sparse representation of the radiation pattern. As a variation from the basis pursuit optimization problem which is widely used in compressed sensing for antenna measurements, a sparsity enhancing weighted l_1-norm minimization problem is considered. The weights are determined from prior information on the antenna from electromagnetic simulations. The proposed method, after investigation with various antennas and comparison with the existing benchmark results in a further reduction of the number of required measurements. A near-optimal sampling technique is adopted to acquire measurement in an incoherent manner for exact recovery of the pattern. The performance of the method has been evaluated using error metrics specific to important parameters of the radiation pattern such as the gain, peak side lobe level and half power beam width. Radiation patterns with non-idealities and distortions have also been recovered with high accuracy from a small number of measurements using the proposed method.

Contents

1

Introduction

1.1. Motivation

Antennas play a crucial role as transducers, facilitating the conversion between guided waves and free space wave propagation in the field of electromagnetics. They are essential components in various wireless communications and sensing systems, including mobile communication, deep space communications, radar technology, radio astronomy, and many more. Often these applications use different antennas designed to satisfy specific requirements (in terms of radiation characteristics) [1][2]. But in certain cases, the design and deployment of the antenna system can lead to imperfections and undesirable deviations from the expected radiation pattern [1].A fundamental and crucial property of any antenna is its radiation pattern, which gives information on the strength of the field radiated by an antenna in a particular direction. For each direction in space, the radiation pattern is characterized by amplitude, phase and polarization. From the measurement of these parameters, the gain, directivity, radiation efficiency and other parameters that affect the system performance can be determined [3]. The monitoring and recording of electromagnetic fields has become increasingly important for assessing the system performance.This makes it essential for testing of the designed antennas before deployment for the corresponding application to ensure optimal performance. Radiation pattern measurement is also necessary in testing of antennas with complex radiating structures which cannot be assessed using simulation tools. This becomes particularly challenging in millimetre(mm) wave applications wherein, for reliable measurements, very stringent conditions imposed on the data acquisition technology in terms of positional accuracy, mechanical tolerances and so on [4]. This property makes antenna radiation pattern measurement a critical step in satisfying the increasing demands from electromagnetic compatibility testing as well as wireless communication technology [5].

In general, radiation pattern measurement procedure required to reconstruct the field and obtain the parameters of interest is a time consuming process [6]. The time complexity increases further depending on the measurement setup considered, antenna bandwidth, type of measurement (near-field (NF) or far-field (FF)) and various other factors. The time of measurement of radiation patterns, assuming a given measurement setup, depends on the number of samples to be measured that enables accurate reconstruction of the field pattern and the acquisition strategy which decides how the data points are acquired [6]. The acquisition strategy greatly depends on the range setup and related mechanical constraints that need to be considered for measurements. The measurement setup/antenna test range can either be indoor or outdoor. In indoor setups, in most cases the pattern measurements take place in an anechoic chamber which is a Faraday cage that greatly reduces the interference from outside sources and reflection of the radiated waves within the chamber thereby allowing accurate assessment of the characteristics of antenna systems. Anechoic chambers may be used for near-field or far-field measurements and typically, the near-field is measured over a dense sampling grid in order

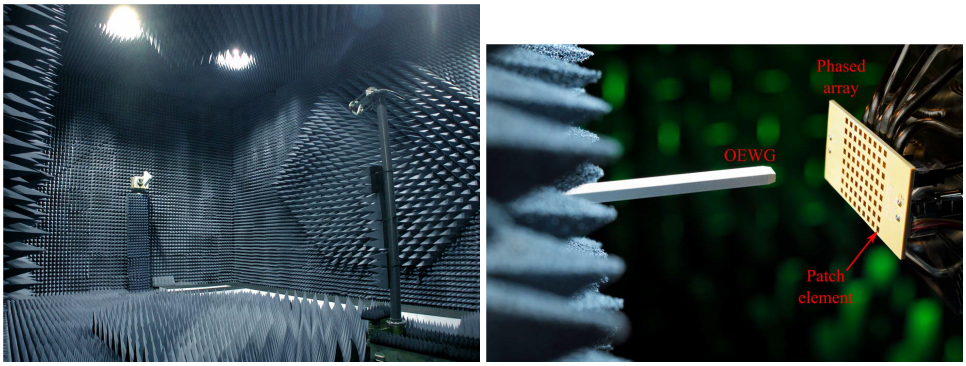

(a) Anechoic chamber measurement setup **(b)** Embedded element pattern measurement [12]

Figure 1.1: Examples of antenna measurement setups

to enable accurate estimation of the far-field from transformation techniques [3]. This increases the number of measurements and consequentially the measurement time. In terms of measurements in the far-field, the sampling step and measurements required depends on the size of the measurement sphere (which depends on the far-field distance from the antenna under test). Measurement of radiation patterns in anechoic chambers is an expensive process where the cost is directly related to the measurement time. For this reason, it will benefit from an economic point of view for industries to use faster measurement technology to achieve the expected accuracy in the reconstructed pattern.

However, depending on the antenna to be tested and the requirement of characterization, the use of anechoic chambers is limited. If the size of the antenna is large, achieving the far-field criteria is not possible in anechoic chambers, which motivates the need for other measurement strategies. For characterization of low frequency, electrically large antennas and arrays for applications in radio astronomy, measurements are performed outdoor using an unmanned aerial vehicle (UAV) [7]. An example of where this is of great relevance is the characterization of arrays and sub-arrays of radio telescope antennas such as the Low Frequency Array (LOFAR) and the square kilometre array (SKA) [8][9]. In these outdoor measurements (especially pertaining to radio telescopes pattern measurement), typically the far-field pattern is estimated using interpolation from a series of pattern cuts with either varying elevation or azimuth [10] whereas in current era of astronomy where various configurations of arrays designed to achieve specific radiation characteristics require three-dimensional radiation pattern measurements which are typically done with flight paths designed for drones in planes at multiple heights [11]. However, the measurement process is limited due to the flying time of drones/UAVs which makes it necessary to find a sampling technique that has lesser sampling locations and fitting the points using a minimum distance path for the UAV to fly in, while still considering positional errors [11].

Another situation which requires faster measurement technology is the requirement to measure embedded element patterns (EEP) of the elements in a phased array which are important to understand the coupling effects that take place in the array due to its topology and influence on the overall radiated field [12]. In 5G millimetre wave (mm-Wave) applications, over-the-air measurements of radiation pattern are very useful to evaluate the performance of both the antenna arrays and the sub-arrays. Arrays with large number of elements mandates the measurement of large number of EEPs, which when a conventional sampling strategy is used for consumes long characterization times. Hence it is desirable to reduce the time of measurement for each EEP which consequentially reduces the overall time required.

Another motivation for developing a sparse sampling technology is for faster array diagnosis where the measured pattern is used to identify errors in the excitation or failure of array elements which lead to undesirable distortions in the resulting array pattern [13] [14]. Faster sampling of the field enables faster and fairly continuous diagnosis of critical systems.

To reduce the measurement time, a faster scanning strategy and a reduced number of measurement samples is required. The technique of compressed sensing can be used in this regard as it is an

effective tool in recovering a signal form greatly under sampled set of measurements [15][16]. This requires the radiation pattern (signal) to be sparse. The antenna radiation pattern however is not sparse directly in the spatial domain in most cases, hence, sparse recovery cannot be directly applied in this case. The pattern can be represented using a sparsifying basis in a different domain (transform domain) where the signal/coefficients exhibit sparsity, which enables the reconstruction of the original signal data using optimization techniques. This reduces the number of measurements greatly compared to the conventional field sampling criteria that have been established in practice. The idea of using CS can be very useful in scenarios where the measurement surface is large requiring many samples and also in near-field measurements which require dense sampling of the NF radiated by the AUT on a spherical surface.

This chapter further explores the state-of-the-art literature on reducing the number of samples required in antenna pattern measurements followed by the identification of certain gaps in the existing work done. Based on the literature review, the research questions of the thesis are formulated.

1.2. Problem Formulation

The main research problem considered in this thesis is to reduce the number of samples/measurements required to characterize the radiation pattern of any given AUT as it is a crucial step before the deployment of an antenna in the wireless system. Reducing the number of samples required to recover the pattern in a given grid will reduce the time required for characterization. The extent to which the number of samples/field measurements required to reconstruct the pattern depends on various factors. A few of them are,

1. Sparsity in the signal (radiation pattern)
2. Choice of transformation basis
3. Sampling strategy
4. Reconstruction method

In the basis pursuit optimization problem, a weighted l_1-norm of the sparse coefficients can be used as an alternative cost function with the motivation of enhancing sparsity in the signal. It is also critical to evaluate the performance of the sparse sampling algorithm to make sure that the recovered pattern is as close as possible to the radiated field at that location in space. The method needs to be verified for a set of AUTs to ensure it is not subjective to a specific type of antenna.

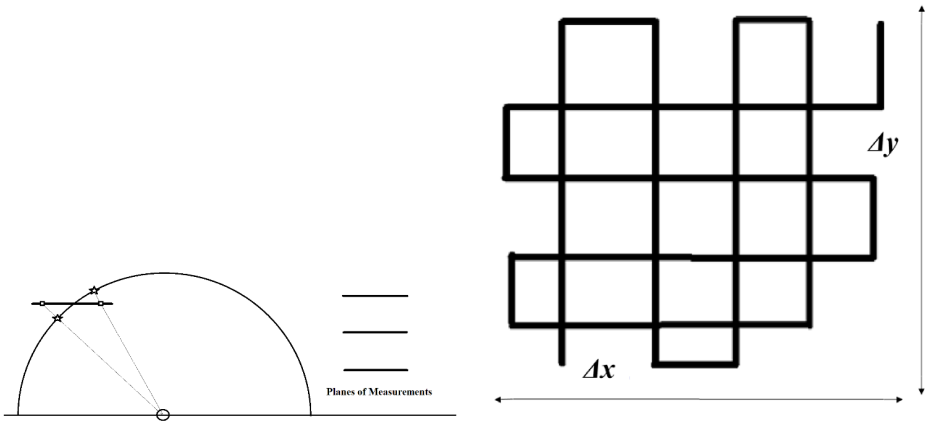

(a) Scanning plane **(b)** Trajectory of the UAV

Figure 1.2: UAV-based antenna pattern measurement [11]

1.3. Scope of Research

It is understood from existing research that in order to reduce the overall measurement time, it includes both reducing the number of samples to be acquired as well as to find an optimal path for probe (range antenna) movement while acquiring the data. The probe movement is constrained by the type of measurement/characterization attempted as well as the mechanical positioning system [17]. The optimization while considering probe movement would involve designing sampling matrices/scan strategies that require less time to acquire data while still providing guarantee of recovery by means of its mutual coherence properties [18][19].

In the work done in this thesis, the probe movement path has not been considered during the design of the sampling technique and the focus is more on finding the optimal (and sparse) set of measurements required to recover a pattern given a specific accuracy. Reducing the number of measurements has an effect on the measurement time as in many cases such as wide band characterization of the AUT, the probe requires a sweep duration to acquire the measurement at a given spatial position before moving to the next sampling location. By reducing the number of samples required, it would scale down the required characterization time. And the problem of finding a minimum distance/time scanning path can be investigated from the reduced set of measurements

The thesis mainly considers electric far-field radiation data (in θ, ϕ) represented in terms of spherical coordinates and the fields are defined on a measurement sphere (surface). However, this can be extended to planar field measurements as well as near-field measurements.

1.4. Literature review

This section contains a brief summary of the state-of-art work done in the area of fast sampling technology for antenna radiation pattern measurements and the research gaps identified in the literature pertaining to the improvement in characterization time of radiation patterns.

1.4.1. State-of-the-art

The radiation pattern of the AUT can either be measured in the far-field where it is straight forward to perform amplitude-only measurements for obtaining the magnitude. But depending on the frequency of operation, physical size and type of antenna,the far-field can be at a far away distance from the antenna which makes 3D characterization a challenging task as specialized measurement environments like anechoic chambers become hard to realize. . To overcome the range issue, it is possible to acquire measurements in the near-field and perform a near-field to far-field transformation (NFFFT) [20]. The drawback is the required number of measurements in the near field to enable the NFFFT and the requirement of both the amplitude and phase of the field at those locations to estimate the far-field from the near-field data. Phase measurements are prone to probe positioning errors in the measurement system which makes phase measurements in the near-field a challenging task [21]. In both cases (NF and FF), a reduction in the number of samples required to find the radiation pattern would reduce the measurement time [22].

Compressed sensing (CS) theory is a way of sparse signal processing that introduces a revolutionary sensing/sampling paradigm which challenges conventional knowledge on data acquisition. According to CS theory, it is possible to recover signals and images that contain a sparse representation using reduced number of samples than traditional methods. Sparsity enables effective fundamental signal processing, such as precise statistical estimation and classification and effective data compression which make it an essential tool for modeling [23]. Compressed sensing has been used in signal processing for various problems such as medical imaging and other sensing applications but recently for over a decade, its potential has also been explored and used in electromagnetic problems such as radar imaging, array diagnosis, antenna measurements and field strength prediction as well [24][25]. Some of the proposed methods to increase the speed of acquisition include sparse sampling of the measurement using ”quadrature analog-to-information conversion (QAIC)” technology [26]. But this

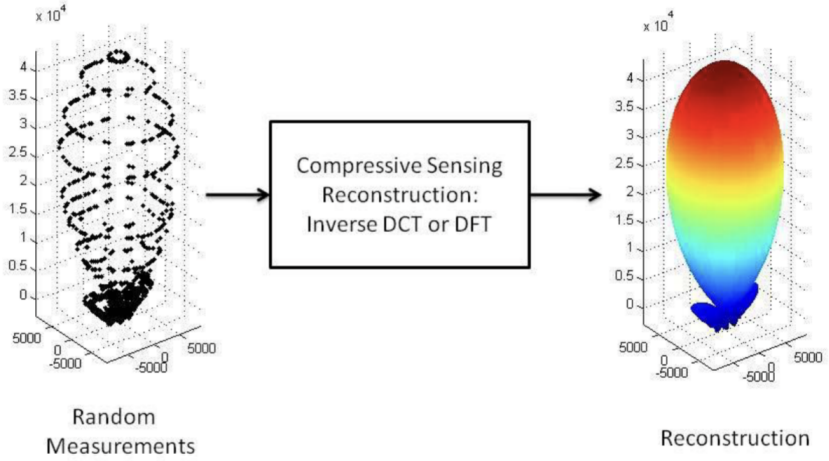

Figure 1.3: Workflow of Compressed sensing based measurements [22]

approach is more at the processing level rather than in the spatial sampling domain.

A better way of reducing the overall measurement time is to reduce the number of samples/measurements over the measurement surface and accurately recover the field from the sparse measurements. In most cases, compressed sensing is applied for the spatial distribution of the electromagnetic field. In certain cases, the radiation pattern of the AUT exhibits sparsity when the discrete Fourier transform (DFT), discrete cosine transform (DCT) or wavelet transform is used as the sparsifying basis [22], [27], [28], [6]. According to work done in [22], DFT matrix based CS provided a better reconstruction of the radiation pattern when compared to DCT matrix. Using DFT as the basis, the radiation pattern was recovered with 20 to 44 % of the total points on the dense sampling grid following dense sampling of $\Delta\theta = \Delta\phi = 1^o$. Another way of representing the antenna electric field is using the spherical harmonic expansion of the field which is based on the theory of acquiring measurements within a sampling sphere [29]. The spherical wave coefficients of the electric field of an antenna would typically have only few non-zero coefficients which makes it a good sparse representation for the 3D radiation pattern. Spherical harmonics have been used in the context of antenna field measurements and reconstruction both in the near-field [30] and in the far-field [29] , [31].

While undersampling the data, it is important to ensure the effect of aliasing artifacts needs to be minimized as much as possible. It is evident that if a uniform/equispaced undersampling of the signal leads to grating lobes in the Fourier transform of the sampling function. The resulting reconstruction of the signal (radiation pattern) exhibits coherent aliasing of the signal components which is undesirable. It is not possible to distinguish between the original signal and its replica [32]. From a compressed sensing point of view, improving the accuracy of recovery means the sensing and sampling basis need to be maximally incoherent with each other [15]. Incoherence can be introduced during sampling by acquiring data in a uniform random manner. This incoherent sampling exhibits interference properties close to that of pure random undersampling wherein the side lobe levels of the response are relatively low which leads to reduced artifacts in the reconstruction. A measure of the mutual coherence between the sensing and sampling bases is the transform point spread function (TPSF). The TPSF is a measure of influence of a single transform coefficient on the other transform coefficients. The sidelobes of the TPSF give an idea of the incoherence present in the selected sampling scheme/trajectory [32].

In case of the acquisition of samples, in literature on using DFT as the sparsity transform, the samples are chosen uniformly at random from the available set of points (with equi-angular separation). The sampling grid considered is a sphere but it can also be a plane or of a different geometry like cylindrical [22]. There are certain sparse sampling schemes suggested while using spherical harmonics as the

basis [29]. The Igloo sampling or Bucci sampling techniques reduces the redundancy in data present in the Hansen/equiangular sampling of the sphere. The samples are selected in random from the grid of measurements according to the decided sampling technique and the selected measurements are used to recover the far-field pattern by solving the basis pursuit problem (l_1 norm minimization).

Adaptive sampling techniques based on the level of variations in the electromagnetic field strength is also discussed in literature. One such approach used to reduce the number of samples required for reconstruction is to use total variation compressed sensing (TV-CS) which aims at minimizing the support of the total variation (gradient) of the signal/underlying function instead of the coefficient vector itself [33]. This is applicable for gradient sparse signals and images. In electromagnetic applications, TV-CS has been used for the electric field strength prediction from less number of measurements by using an adaptive field sampling strategy (sequential experimental design) and using the chosen samples in the TV-CS algorithm [34] [35]. The sequential experiment design is a method to model the number and values of inputs from its domain for simulations of systems to use the set of outputs/measurements to predict the underlying function. Given a function f(x,y), it depends on sampling the field/ function (i.e. finding (x,y)) such that it maintains a balance between exploration and exploitation using a hybrid cost function. The most commonly used algorithm to design this sampling strategy is the LOLA-Voronoi algorithm [36]. Voronoi tessellation is used to explore the function space by acquiring samples from least explored regions and the local linear approximation algorithm is used to estimate the gradient of the function and identify the highly non-linear regions based on the provided sampling locations.

The hybrid cost function is given by

$$H\left(\mathbf{p}_i\right) = V\left(\mathbf{p}_i\right) + \frac{E\left(\mathbf{p}_i\right)}{\sum_{j=1}^{n} E\left(\mathbf{p}_j\right)} \tag{1.1}$$

where $V\left(\mathbf{p}_i\right)$ is the Voronoi cell size/volume decided by the number of closest neighbours to the selected sample and $E\left(\mathbf{p}_j\right)$ is the non-linearity measure computed assigned for each selected point $\mathbf{p}_i$. If **f** is the field data, **y** is the measurements vector and Φ is the MxN observation operator whose $(m,n)^{th}$ entry is set to Φ_{mn}=1 if the field is probed at the location m.

$$\hat{\mathbf{f}} = arg\{\min_{\mathbf{f}} \|\nabla \mathbf{f}\|_1\} \tag{1.2}$$

This adaptive sampling strategy is well suited for TV-CS as it performs better than random acquisition of field measurements but it depends on the gradient sparsity of the field rather than transform sparsity.

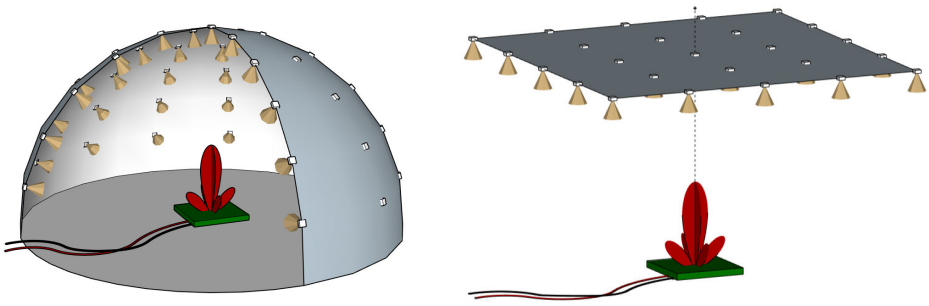

(a) Example of spherical measurement array **(b)** Example of planar measurement array

Figure 1.4: Fixed measurement setup [37]

Another measure of the incoherence would be the Gram matrix, whose first row gives the point spread function for a selected sampling scheme. The entries of Gram matrix can be selected for optimizing the point spread function and consequentially optimizing the sampling vector which dictates how the samples are acquired [38]. The optimization is done with respect to the sampling matrix as the sparsifying basis is chosen beforehand, the maximum off-diagonal entry in the Gram matrix is the cost function in this case, and this can also be represented as minimizing the norm difference between

Gram matrix and the identity matrix [39]. The difference between the work done in [39] and its extension to the antenna radiation pattern measurement problem is that the measurement vector is a binary vector where 1 denotes if a measurement is acquired and 0 if the sampling point is not considered.

From most existing literature, it is noted that sampling matrices with random entries (based on Gaussian/Bernoulli distribution) are known to satisfy the restricted isometry property (RIP) with very high property hence allowing accurate recovery of the underlying radiation pattern data. If the field is sampled along a sphere, a visualization of equiangular sampling and random sampling over the radiation sphere is shown in the below figure.

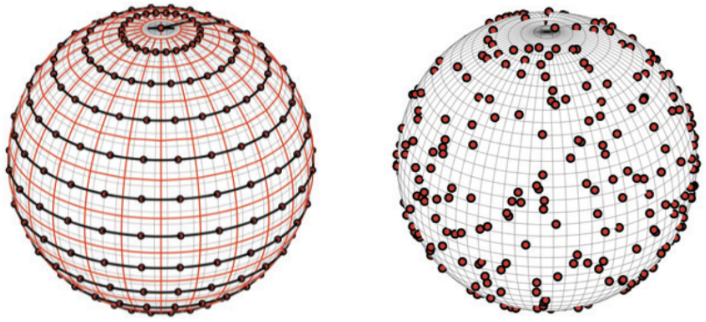

(a) Equi-angular sampling over a sphere

(b) Cosine weighted random undersampling over a sphere

Figure 1.5: Scan methods to acquire samples over a sphere [17]

In [17], it is mentioned that in order to reduce the probe movement time while scanning for measurements along a sphere, fixed sampling schemes are used to compute the mutual coherence with the sparsifying basis (which is the spherical harmonic expansion). If they are incoherent, the resulting compressed sensing matrix would ensure accurate recovery provided the number of measurements obey the theory of compressed sensing, which will be explained in the next chapter.

Currently the most commonly used methods to solve the CS recovery problem is either to use greedy algorithms such as orthogonal matching pursuit (OMP), CoSAMP etc. to solve the l_0 minimization problem or to formulate l_1 minimization as a basis pursuit problem [15] [23]. Another approach from literature to enhance the sparsity is by using weighted l_1 minimization compared to the basis pursuit formulation which uses l_1 norm of the coefficients as the cost/objective function [40]. To explain in a simple manner, in l_1 minimization the large coefficients are penalized more heavily than smaller coefficients which tends to regulate the values of large coefficients. In weighted l_1 minimization, typically the weights chosen are inversely related to the underlying coefficients in the data, which gives lesser weights to higher value coefficients. It provides a sort of regularization to the objective function[41].

1.4.2. Gaps in literature

From the literature review on the work done on faster measurements for antenna radiation pattern characterization, it is emphasized that reducing the number of samples and optimizing the sampling strategy for obtaining sparse measurements to recover the pattern is a key aspect of reducing time of characterization. In previous work, the best sampling strategy or the optimal number of measurements to achieve a desired accuracy in measurements are decided based on recovery criteria established by compressed sensing theory [16]. This includes near-optimal sensing matrices that satisfy the restricted isometry property with high probability or computing the mutual coherence of the CS matrix for a given/selected sampling matrix [42][43]. However, to the best of my knowledge, current existing work done in literature does not make use of the simulated radiation pattern information which is available prior to measurement in most relevant scenarios. The ideal pattern which is expected from a designed antenna under test (AUT) can be determined through electromagnetic simulations, provided the design fits to the requirements of electromagnetic solvers. Current fast sampling/measurement

techniques only assume sparsity in the pattern and do not use any other prior information on the AUT to further optimize the measurement method. Most of the available research on antenna measurements using compressed sensing have made use of sampling of the electric near field of the antenna and used the spherical wave expansion as the transform basis as the number of mode coefficients required to represent an electromagnetic field is usually sparse. The discrete Fourier transform has also been used as a sparsifying representation basis for far-field patterns but it has not been explored or evaluated in detail for different types of antenna patterns. Another key aspect that has not been explored in literature is the recovery of the sparse coefficients of a given radiation pattern using sparsity enhancing compressed sensing techniques such as having the weighted l_1-norm as the objective function of the optimization problem rather than the conventionally used l_1-norm.

To summarize, the gaps identified in existing literature are listed below

1. Prior information on the AUT from electromagnetic simulations have not been used in optimizing the measurements
2. The use of sparsity enhancing recovery methods in CS have not been explored in the context of radiation pattern measurements
3. Most recovery methods are evaluated only using the mean squared error metric and no other specific parameters of the radiation pattern are focused on during performance evaluation.
4. An evaluation of performance of the CS based measurement strategies have not been performed for non-ideal radiation patterns (with errors and distortions).

1.5. Research objectives

Deriving from the problem formulation and literature review, it is essential to establish the research objectives of thesis. From the state-of-the-art work done on radiation pattern measurements using compressed sensing, the spherical harmonics and DFT have been identified as good sparsifying bases for the pattern. Hence, both sparsifying basis functions are used to perform compressed sampling and reconstruction of the antenna pattern from sparse measurements. Since the weighted l_1-norm minimization based recovery that enhances sparsity in the data has not been applied in the context of CS for electromagnetic applications, it is decided to investigate the new method to understand its performance in reducing the number of measurement.

1. Find a well-suited sparse basis representation for far-field antenna patterns
2. Identify the near-optimal sampling scheme to acquire measurements
3. Use prior information of antenna to investigate the use of weighted l_1 norm minimization for better recovery of radiation pattern
4. Compute variation of different aspects of the radiation pattern by comparing specific parameters of the ground truth and the reconstructed pattern.
5. Test the robustness of the method to measurement noise and other effects on the pattern.

1.6. Novelties in the thesis

The novelties explored in this thesis to obtain faster measurements is listed below.

1. Prior information on the antenna is used with a weighted l_1-norm as objective function in the CS recovery problem for the first time in the context of antenna radiation pattern measurements.
2. A systematic study of the DFT as a sparsifying basis has been performed for the first time.
3. A comparison between compressed sensing using DFT and spherical harmonics is investigated.
4. The performance of algorithms has been evaluated using a customized set of error metrics in addition to the widely used comparison metric, the mean squared error (MSE).
5. Various distortions are introduced to the antenna radiation pattern and the performance of the algorithms on the distorted patterns are studied.

1.7. Thesis structure

The thesis has started with the introduction and the state-of-the-art work done on the problem statement considered. The novelties have been decided based on the identification of research gaps in existing literature. Chapter 2 provides the necessary theoretical background on antenna pattern measurements and compressed sensing techniques. Chapter 3 explains the signal model adopted for the CS problem, the recovery methods considered, construction of the sampling matrices. Chapter 4 is about sparse recovery of patterns by solving the l_1 (benchmark) and weighted l_1 (new method) minimization problem for both the DFT as well as spherical harmonic basis. Furthermore, non-idealities have been introduced in the radiation pattern to test the method's performance on distorted antenna patterns. Finally, error metrics specific to certain aspects of the radiation pattern (gain, HPBW, PSLL). The sampling strategy can be further optimized based on the selecting the strategy that gives the minimum error in one of the quantities. Along with the results of reconstruction, the various error metrics that have been introduced to assess the performance of recovery have also been discussed and their results presented thereby. To do this, both antenna radiation patterns simulated using MATLAB and data measured from tests on an AUT performed at the Microwave Sensing Signals and systems (MS3) group are used.

2

Theoretical Background

This chapter will provide the necessary background theoretical information on the concepts and techniques involved with the thesis. The chapter has been organized into two sections. Section 2.1 gives an overview of antenna measurement techniques, radiation patterns and the parameters of importance. A brief introduction to the theory of compressed sensing, the algorithms and methods well suited for sparse recovery of the signal and the information on the transform basis functions used are discussed in section 2.2.4

2.1. Antenna measurements

Measurement of the transmit and receive mode properties of antennas is a critical step before they are put to use in any application. The standard test practices for antenna measurement assume the AUT is a passive, linear and reciprocal device. Due to the property of reciprocity, the transmit and receive characteristics of the AUT are similar, thus enabling measurements in either mode. It is also crucial to decide on the range setup

2.1.1. Measurement techniques and setups

Antenna ranges are developed for measuring radiation patterns of antennas and contains the necessary instrumentation and physical space required for the measurement process. The basic categories of types of ranges are

- Free-space ranges
- Ground reflection ranges
- Near-field ranges

Typical ranges come under the free-space range and are classified as: the elevated range, the compact range, and most anechoic chambers. Ideally the measurements are done with both the AUT and range antenna in the far-field of the other antenna. In certain cases when the AUT is electrically large, the far-field condition ($R > 2D^2/\lambda$) cannot be achieved in the free-space range setup and in that case, near-field measurements are a better suited option and the far-field pattern can later be obtained by performing a near-field to far-field transform (NFFFT).

A range antenna and an AUT are shown in the diagram. The positioning subsystem directs the movement of the antennas. The transmit subsystem generates the desired test frequency, while the receive subsystem detects the AUT response at various aspect angles. The workstation manages the entire data collecting process and reports back to the operator. The measurement systems of antennas use scalar or vector devices in the instrumentation

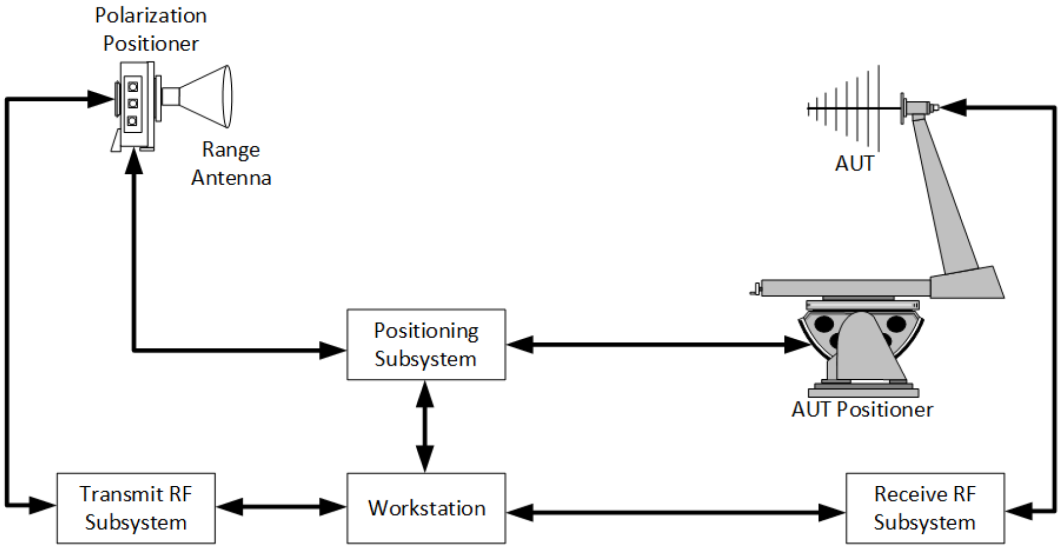

Figure 2.1: Block diagram of a typical antenna-measurement system [3]

2.1.2. Radiation pattern and its characteristics

The radiation pattern is a fundamental property of an antenna/array that describes the spatial distribution of the electromagnetic field and exists over a full radiation sphere surrounding the antenna. The most common type is the normalized gain or directivity pattern plotted on a decibel (dB) scale versus angle. Recent advances in antenna and array design technologies for various applications such as 5G base stations, radio telescopes etc. make use of antenna radiation with bean scanning, beam squint and irregular radiation patterns to achieve desired performance metrics. In most cases, the radiation pattern represents the gain or directivity or electric field defined over a sphere. It varies as a function of azimuth (ϕ) and elevation (θ) angles.

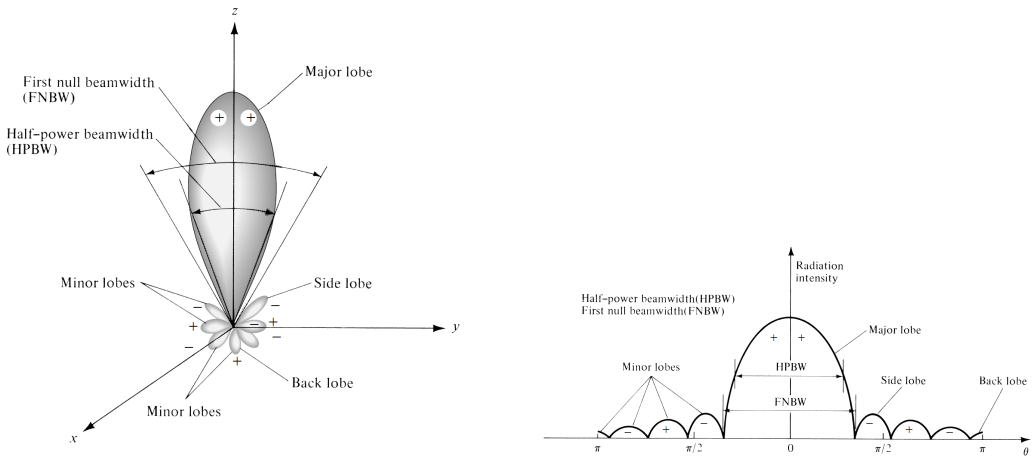

(a) Radiation pattern and lobes

(b) Linear plot of power pattern

Figure 2.2: Antenna radiation pattern parameters [1]

The electric far-field $\vec{E}$ at any observation point in space is defined as

$$\vec{E}(\vec{r}) = \frac{e^{-jkr}}{r}\vec{F}\left(\hat{a}_r\right) \tag{2.1}$$

where $\vec{r}$ is the position vector of the point in free space where the field is defined at, k is the wave number, and $\vec{F}$ is the far-field pattern function which depends only on the direction of the observation point ($\hat{a}_r$).

Other quantities of interest from the radiation pattern are the gain, half power beam width, peak side lobe level and the average side lobe levels.

2.2. Compressed sensing

If the majority of the components of a signal are zero, it is said to be sparse. Many real-world signals, as objectively recorded, are compressible in the sense that they are well approximated by sparse signals—often after a suitable change of basis. JPEG, for example, depends on image sparsity in the discrete cosine or wavelet basis to achieve compression by saving only the largest discrete cosine or wavelet coefficients. The remaining coefficients are all set to zero.

2.2.1. Introduction

Looking more closely at the basic compressed sensing problem of reconstructing a sparse vector $\mathbf{x} \in \mathbb{C}^N$ from under determined data $\mathbf{y} = \mathbf{Ax} \in \mathbb{C}^{m \times N}$, two questions emerge:

- How should the linear measurement procedure be designed? In other words, which matrices A CmN are appropriate?
- How does one deduce x from y = Ax? To put it another way, what are efficient reconstruction algorithms?

These two questions are not fully independent, because the reconstruction method must take A into consideration, but we will demonstrate that the study of the matrix A may frequently be separated from the analysis of the algorithm.

The observed data $y \in \mathbb{C}^M$ is mathematically related to the signal $\mathbf{x} \in \mathbb{C}^N$ of interest by Ax = y. The linear measurement (information) process is represented by the matrix $\mathbf{A} \in \mathbb{C}^{m \times N}$. Then, by solving the above linear system, one attempts to recover the vector $\mathbf{x} \in \mathbb{C}^N$. According to conventional knowledge, the number m of measurements, or the amount of measured data, must be at least as large as the signal length N (the number of x components).

This idea underpins the majority of modern technology, including analog-to-digital conversion, medical imaging, radar, and mobile communication. Indeed, if m < N, classical linear algebra implies that the linear system (1.1) is under determined and that there are an unlimited number of solutions (assuming, of course, that at least one exists). In other words, in this scenario, it is impossible to extract x from y without further information. This fact is also related to the Shannon sampling theorem, which stipulates that the sampling rate of a continuous-time signal must be twice its highest frequency in order for reconstruction to be possible.

This problem of finding a solution for an under determined system of equations can be solved using the theory of compressed sensing which makes use of the underlying sparsity in the signal

2.2.2. Mathematical formulation of compressed sensing

The sparse/compressed sensing problem of recovering a sparse vector $x \in \mathbb{C}^n$ from a set of linear measurements defined by $\mathbf{y} = \mathbf{Ax} \in \mathbb{C}^m$ where the number of measurements m<N, can be solved by solving the optimization problem in

$$\hat{\mathbf{x}} = \min_{\mathbf{x} \in \mathbb{C}^N} \|\mathbf{x}\|_0 \text{ s.t. } \mathbf{y} = \mathbf{Ax} \tag{2.2}$$

But the $||.||_{l_0}$ minimizing optimization problem is an NP hard problem due to its non convexity thus allowing only the use of greedy algorithms like orthogonal matching pursuit (OMP), CoSAMP, etc. Luckily, a convex relaxation of the objective function $f_0(\mathbf{x}) = ||(x)||_0$ can be performed to replace it by the

function $f_0(\mathbf{x}) = ||(x)||_l$ where $0 \leq l \leq 1$. When $l = 1$, the objective becomes a convex function (as l_1 norm is convex) and the problem can be reformulated as

$$\hat{\mathbf{x}} = \min_{\mathbf{x} \in \mathbb{C}^N} \|\mathbf{x}\|_1 \text{ s.t. } \mathbf{y} = \mathbf{A}\mathbf{x} \tag{2.3}$$

The new problem formulation is known as Basis pursuit and can be solved using currently available solvers or convex optimization such as CVX, YalMIP, SPGL1 etc. The problem in 2.3 guarantees accurate recovery of the sparse signal provided the null space property, which is a necessary and sufficient condition for exact recovery is satisfied. We designate by $\mathbf{v}_S$ the vector in $\mathbb{C}^S$ that is the limitation of $\mathbf{v}$ to the indices in set $S \subset [N]$, or the vector in $\mathbb{C}^N$ that coincides with $\mathbf{v}$ on the indices in S and is extended to zero outside S, for a vector $\mathbf{v}$ and a set S.

A matrix $\mathbf{A} \in \mathbb{K}^{m \times N}$ is said to satisfy the null space property relative to a set $S \subset [N]$ if

$$\|\mathbf{v}_S\|_1 < \|\mathbf{v}_{\overline{S}}\|_1 \text{for all } \mathbf{v} \in \ker A \setminus \{\mathbf{0}\} \tag{2.4}$$

The restricted isometry property is another type of property that assures reliable recovery of the sparse signal. The restricted isometry property, also known as the uniform uncertainty principle, is a tighter measure of analyzing the quality of a measurement matrix to provide a more comprehensive analysis for varied sparsity levels. The s^{th} restricted isometry constant $\delta_s = \delta_s(\mathbf{A})$ of a matrix $\mathbf{A} \in \mathbb{C}^{m \times N}$ is the smallest $\delta \geq 0$ such that

$$(1 - \delta)\|\mathbf{x}\|_2^2 \leq \|\mathbf{A}\mathbf{x}\|_2^2 \leq (1 + \delta)||\mathbf{x}||_2^2 \tag{2.5}$$

for all s-sparse vectors $\mathbf{x} \in \mathbb{C}^N$. Its equivalent expression is provided below.

$$\delta_s = \max_{S \subset [N], card(S) \leq s} \|\mathbf{A}_S^* \mathbf{A}_S - \mathbf{Id}\|_{2 \to 2} \tag{2.6}$$

The measurement matrix $\mathbf{A}$ satisfies the restricted isometry property with isometry constant δ_s, if δ_s us small for reasonable large sparsity levels s [16]. But verifying both these properties is a computationally complex problem for each measurement matrix generated. For this reason, the coherence of the measurement matrix is considered as a metric to ensure signal recovery using matching pursuit, basis pursuit and thresholding algorithms.

The goal for good recovery using compressed sensing is that the columns of the measurement matrix must be maximally incoherent with each other. Mathematically, the coherence $\mu = \mu(\mathbf{A})$ of a matrix $\mathbf{A}$ is given by

$$\mu := \max_{1 \leq i \neq j \leq N} |\langle \mathbf{a}_i, \mathbf{a}_j \rangle| \tag{2.7}$$

where $\mathbf{a}_1, \mathbf{a}_2, ..., \mathbf{a}_N$ are the l_2-normalized columns of the matrix $\mathbf{A} \in \mathbb{C}^{m \times N}$, i.e. $\|\mathbf{a}_i\|_2 = 1$ for all $i \in [N]$

The maximum value coherence of $\mathbf{A}$ can take is $\mu = 1$. The minimum value of μ is termed Welch bound. The lower bound for coherence is given as

$$\mu \geq \sqrt{\frac{N - m}{m(N - 1)}} \tag{2.8}$$

The Welch bound is achieved under the condition that the columns of $\mathbf{A}$ i.e. $\mathbf{a}_1, \mathbf{a}_2, ..., \mathbf{a}_N$ form an equiangular tight frame. The Gram matrix given by $\mathbf{G} = \mathbf{A}^* \mathbf{A} \in \mathbb{K}^{N \times N}$

2.2.3. Weighted l_1-norm minimization

Another method to further enhance the sparsity present in data is to use a weighted/re-weighted l_1-norm minimization which considers a weighted l_1 norm as the cost/objective function.

Let $\mathbf{w}$ be the set of weights used in the optimization problem, where each entry of the vector w_1,w_2,....,w_N are positive entries.

$$\min_{x \in \mathbb{R}^n} \sum_{i=1} w_i \, |x_i| \qquad \text{subject to } y = \Phi x \tag{2.9}$$

If the weights are chosen as the inverse of the sparse signal or coefficients **x** to be recovered, it provides the most efficient recovery and also reasonably rectifies a key difference between the l_0 and l_1 norm which arises due to the convex relaxation. In the l_0-norm, only the sparsity of the signal is considered a cost, whereas in the l_1-norm, the cost value depends directly on the magnitude of the signal/coefficient value which is not the best objective function possible.

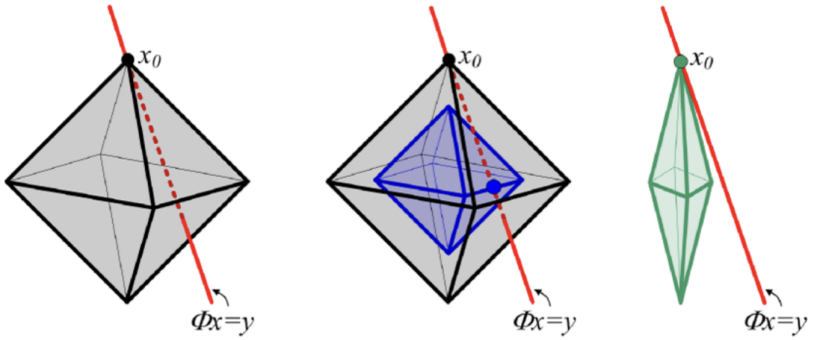

Figure 2.3: Weighted l_1 minimization improving sparse signal recovery - geometric interpretation [40]

Fig. 2.3 shows a visualization of the feasible set and the l_1-norm ball, whose intersections contribute to a solution. It shows that weighted l_1-norm allows for finding a unique solution by solving the modified optimization problem (provided the recovery criteria according to CS hold good).

2.2.4. Basis functions for sparse representation

Compressed sensing is applicable to various electromagnetic problems such as antenna array diagnosis, and antenna pattern measurements. This is from exploiting the underlying sparsity present in the radiation pattern data in the suitable transform basis. Sparsity in the transform coefficients of the pattern enable use of compressed sensing to reduce the number of samples required by employing incoherent measurement strategy.

A few of the basis dictionaries that can be useful for antenna measurements is explained in this subsection.

Discrete Fourier Transform

The discrete Fourier transform (DFT) provides a translation of a given signal to the frequency domain. In other words, it expresses a given signal as a linear combination of complex sinusoids of different frequencies. The DFT of a finite discrete signal **x**[**n**] is given by

$$\mathbf{X}(K) = \sum_{n=0}^{N-1} \mathbf{x}[n] e^{-j2\pi ft} \tag{2.10}$$

where $\mathbf{X}(k)$ represents the DFT coefficients of the signal. The N-point DFT of a signal can be expressed as $\mathbf{X} = \mathbf{W}\mathbf{x}$ where **X** is the DFT coefficients. **x** is the signal samples and **W** is the NxN square DFT matrix given by

$$\Psi = \mathbf{W}_N = \begin{bmatrix} 1 & 1 & 1 \cdots & 1 & \\ 1 & W_N & W_N^2 & \cdots & W_N^{N-1} \\ & W_N^2 & W_N^4 & \cdots & W_N^{2(N-1)} \\ \vdots & \vdots & \vdots & \cdots : & \vdots \\ 1 & W_N^{N-1} & W_N^{2(N-1)} & \cdots & W_N^{(N-1)(N-1)} \end{bmatrix} \tag{2.11}$$

where $W_N = e^{j2\pi N}$ and N is the total length of the signal.

The DFT matrix $\Psi = W_N$ satisfies the required properties of unitary matrix with each column orthogonal to the other (orthonormal basis).

Spherical Harmonics expansion

The radiation pattern is usually defined on a spherical surface in most cases, thereby enabling the field can be represented as a linear combination of spherical harmonics (illustrated in Fig. 2.4. According to theory, most electromagnetic fields exhibit sparsity in their spherical wave coefficients which makes this well suited for compressed sensing in antenna pattern measurements [44][29].

$$E(\theta, \varphi) = \sum_{l=0}^{\infty} \sum_{m=-l}^{l} c_{lm} Y_l^m(\theta, \varphi) \tag{2.12}$$

where c_{lm} are the spherical wave coefficients of degree l and order m, $\mathbf{Y}_l^m(\theta, \phi)$ is the value of the spherical harmonic corresponding to the value of l and m, computed at the position (θ, ϕ).
The spherical harmonics can be computed using the expression

$$Y_l^m(\theta, \varphi) = \sqrt{\frac{(2l+1)(l-m)!}{4\pi(l+m)!}} P_l^m(\cos\theta) e^{\mathrm{Im}\,\varphi} \tag{2.13}$$

where P_l^m represents associated Legendre polynomials. The spherical harmonic functions for negative order (m<0) are computed using the conjugate property of spherical harmonic functions.

$$\mathbf{Y}_l^{-m}(\theta, \phi) = (-1)^m \mathbf{Y}_l^{m*}(\theta, \phi) \tag{2.14}$$

In practice, since an infinite summation is computationally complex, a truncation order for the value of L is defined as $L = (2\pi/\lambda)a$ where λ is the wavelength of the electromagnetic wave generated, a is the radius of the smallest sphere enclosing the radiating structure of the AUT.

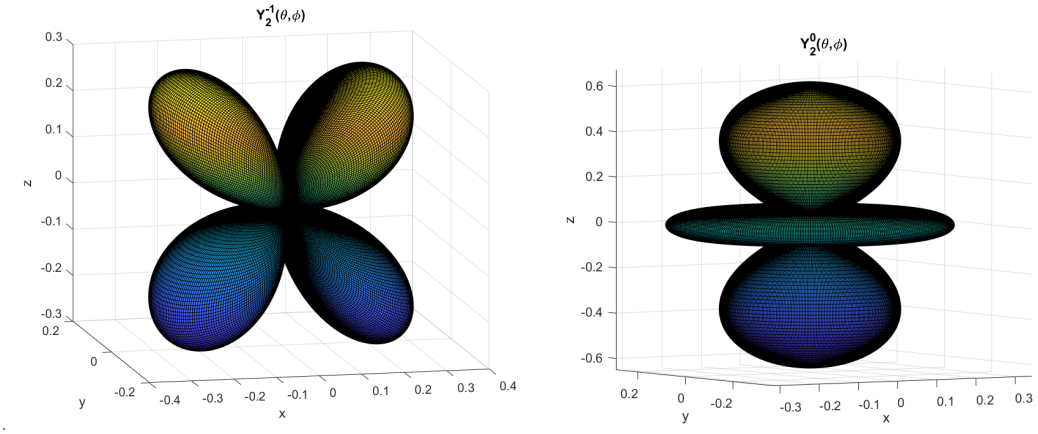

(a) Spherical Harmonic of degree l=2, order m = -1

(b) Spherical Harmonic of degree l=2, order m = -1

Figure 2.4: Spherical harmonic functions visualization

3

Simulation Setup

This chapter will give a brief overview about the way in which the simulation was carried out, the assumptions made and how the data model, error parameters to evaluate performance and the optimization methods are explained. The sparse representation of the radiation patterns is obtained using the DFT and spherical harmonic expansion of the electric field data. The measurements acquired are used in the optimization problem to find the sparse coefficient vector minimizing the cost of the objective function. Based on the objective function the quality of recovery can cary. In the work presented, the l_1-norm and weighted l_1-norm of the coefficient vector is chosen as the weight and their performances are compared. The mathematical formulation of the signal model, sampling technique and optimization problem are explained in this chapter elaborately.

3.1. Signal Model

The antenna radiation pattern is considered as a signal varying as a function of space, depending on the coordinate system considered. Let $E(\theta, \phi)$ be the electric field pattern represented as a matrix with rows representing variation in elevation (θ) and columns representing variation in azimuth (ϕ) angles. Consider the pattern to be vectorized as a signal vector of the form $f(\theta, \phi)$. The signal is assumed to have a sparse representation in a particular transform domain corresponding to a sparsifying basis Ψ. In the work done in this thesis, the Discrete Fourier transform (DFT) and spherical harmonic functions are chosen as the sparsifying transform basis.

The signal measurements can be denoted as

$$y(\theta, \phi) = \mathbf{y} = P_\Omega(f(\theta, \phi)) = \Phi\mathbf{f} \tag{3.1}$$

where P_Ω represents the sub-sampling operator and Φ is the sampling or measurement matrix which dictates how many samples are measured/considered to recover the field data.

The radiation pattern is not sparse in its signal domain (function of space) whereas many antenna patterns exhibit sparsity once transformed to a different domain.
The far-field can be expressed as a linear combination of the basis functions given by

$$f(\theta, \phi) = \mathbf{f} = \Psi\mathbf{x} \tag{3.2}$$

For the DFT as transform basis, the DFT matrix **W** is the basis matrix $\mathbb{X}$. When the spherical harmonics are used, the measurement matrix **A** for the desired specified directions $(\theta_i, \phi_i), \forall i \in M$ is given as

$$\mathbf{A} = [\mathbf{Y_0^0}(\theta,\phi) \quad \mathbf{Y_1^{-1}}(\theta,\phi) \quad \mathbf{Y_1^0}(\theta,\phi) \quad \mathbf{Y_1^1}(\theta,\phi).....\mathbf{Y_L^{-L}}(\theta,\phi).....\mathbf{Y_L^L}(\theta,\phi)] \tag{3.3}$$

where $\mathbf{Y_l^m}(\theta,\phi)$ represents the vector spherical harmonic of degree l, order m computed at the locations defined by θ and ϕ.

The inverse relation gives the required coefficients which exhibit sparsity ($||\mathbf{x}||_0 = s << N$)

$$\mathbf{x} = \Psi^{-1}\mathbf{f} \tag{3.4}$$

If we consider the sparse representation of the signal in the measurement model, the resulting expression is

$$\mathbf{y} = \Phi\Psi\mathbf{x} + \mathbf{n} = \mathbf{A}\mathbf{x} + \mathbf{n} \tag{3.5}$$

where **A** is known as the compressed sensing matrix (order M x N).

A flowchart representing the signal processing pipeline is shown in Fig. 3.1.

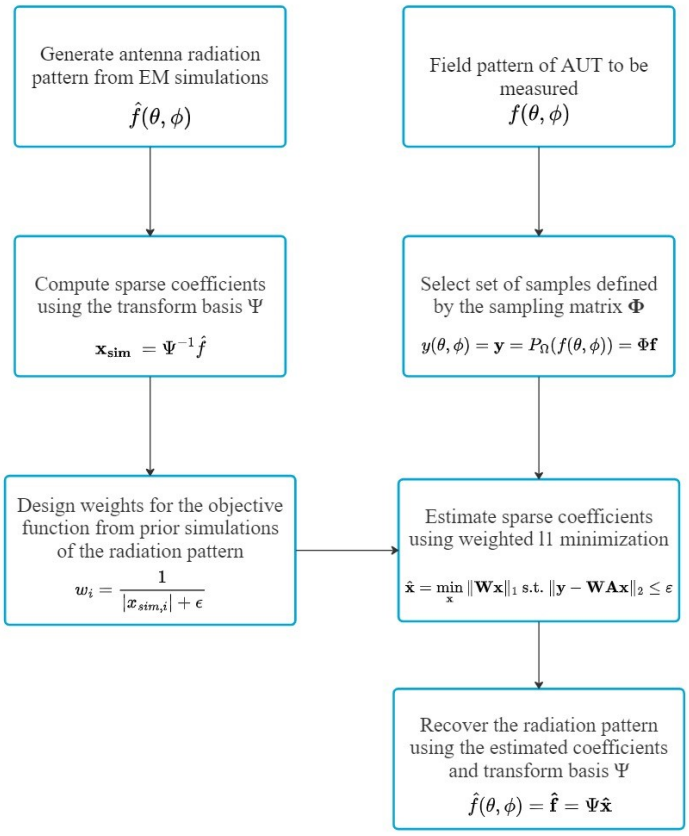

Figure 3.1: Data processing pipeline shown as a flow chart

If the measurement matrix Φ performs subsampling on the data, the matrix has exactly M ones and rest of the entries are zero. Each row must contain 1 at the index where the field is sampled at. The requirement for compressed sensing to give an accurate reconstruction of the field pattern (signal) is that the matrix **A** must follow restricted isometry property with a small value for the RIP constant [15]. But in a practical scenario, verifying the restricted isometry property is a very hard problem. Instead, it is shown in articles that random partial Fourier matrices obey RIP with a high probability and act as effective CS matrices. A random partial Fourier matrix (RPFM) corresponds to selecting a specific number of rows (M rows) of the DFT matrix, which indirectly implies selecting samples at random (using a

certain distribution) from the far-field pattern/signal.

Using basis pursuit to recover the sparse coefficients of the signal is the current benchmark for using compressed sensing in antenna pattern measurements and the recovery problem is formulated as shown in 3.6

$$\hat{\mathbf{x}} = \min_{\mathbf{x}} \|\mathbf{x}\|_1 \text{ s.t. } \|\mathbf{y} - \mathbf{A}\mathbf{x}\|_2 \leq \varepsilon \tag{3.6}$$

where $\hat{\mathbf{x}}$ is the estimated signal coefficients from the field measurements $\mathbf{y}$. ϵ is the maximum tolerable error between the measurements and the recovered signal estimate. In a noiseless reconstruction scenario $\epsilon = 0$.

In order to improve the enhance the usage of sparsity in the recovery process, weighted l_1 norm minimization procedure is employed where the weighted l_1 norm is the objective function in the optimization problem, formulated as

$$\hat{\mathbf{x}} = \min_{\mathbf{x}} \|\mathbf{W}\mathbf{x}\|_1 \text{ s.t. } \|\mathbf{y} - \mathbf{W}\mathbf{A}\mathbf{x}\|_2 \leq \varepsilon \tag{3.7}$$

where the diagonal weight matrix **W** = diag(**w**) is obtained from the weights assigned to each coefficient. In most cases, there is not a lot of information about the signal to be measured and recovered. But in terms of antenna radiation pattern measurements, the expected radiation pattern for a given AUT is available through electromagnetic simulations from 3.4. The coefficients from the simulated radiation pattern can be used to construct the weights to apply in the modified recovery problem.

The weights considered for this problem are of the form as shown in 3.8

$$w_i = \begin{cases} \frac{1}{|x_{0,i}|+\epsilon}, & x_{0,i} \neq 0 \\ \infty, & x_{0,i} = 0 \end{cases} \tag{3.8}$$

where $\mathbf{x}_0$ is the coefficients of the ideal/simulated pattern and ϵ is a tolerance parameter to allow the possibility for non-zero coefficients apart from the support of $\mathbf{x}_0$ in the event of measurement errors in the AUT.

Another method that does not assume the availability of prior information about the coefficients is the re-weighted l_1 norm minimization problem.

The re-weighted l_1 norm minimization does not require any prior information from the AUT. Instead, it enhances the sparsity present in the data through means of the modified optimization problem (with the weighted l_1 norm as the objective function) where the weights are calculated iteratively from the estimate of coefficients at each iteration. The algorithm can be explained as follows.

1. Set the initial weights (at iteration i=1) $\mathbf{w}^{(l)} = \mathbf{1}$ and W = diag(w).
2. Solve the optimization problem given by eqn. 3.7
3. The estimated coefficients $\mathbf{x}^{(l)}$ are used to update the weights vector as $w^{(i+1)} = \frac{1}{|x_i^{(l)}|+\epsilon}$, where i=1,....,N
4. The iterative procedure is terminated after a pre-determined number of iterations l_{max}.

The parameter $\epsilon > 0$ ensures that the weight function still allows the recovery of coefficients beyond the support of the coefficients. This is done as to accomodate the occurrence of changes in the sparse coefficients that may be a consequence of changes in the antenna radiation pattern (in this context) which is the signal/quantity to be measured.

In order to evaluate the performance of the method, the sampling and recovery technique has been applied to simulated and archival data from measurements. Most of the antenna radiation patterns used have been designed and simulated using Antenna Toolbox in MATLAB.

The Antenna toolbox is used to create a required antenna object corresponding to a specific type of antenna (dipole, patch, dielectric resonator antenna, linear and planar arrays etc.) and the desired parameters. Some of the important design parameters in MATLAB for an antenna are

1. Operating Frequency
2. Physical Dimensions
3. Material Properties
4. Feed Type
5. Element spacing (arrays)
6. Number of elements (arrays)

The electric and magnetic fields of the designed antenna can be computed using their corresponding function in MATLAB. An example of the radiation pattern of a pyramidal horn that was simulated as part of the work and used in further stages to evaluate the method, is shown in the figure below.

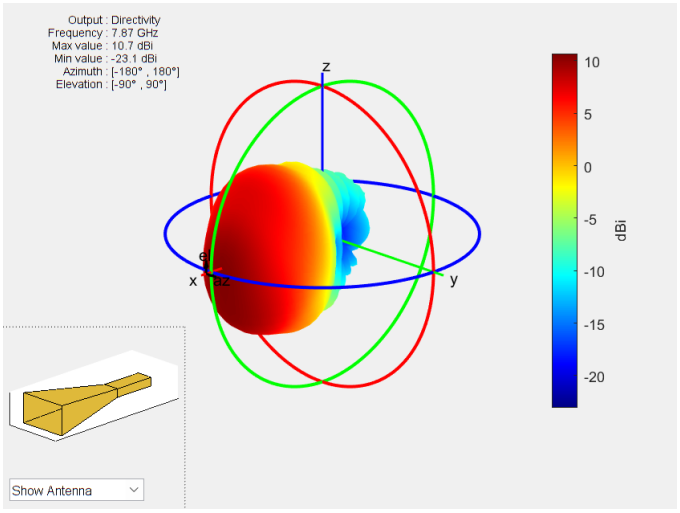

Figure 3.2: 3D radiation pattern of a pyramidal horn antenna operating at 7.87GHz designed using MATLAB

In a similar manner few more antenna patterns have been obtained and used to validate the results of the sampling and recovery method. In the shown radiation pattern, the measurements are field samples acquired at specific field locations in azimuth and elevation in spherical coordinates (θ, ϕ).

3.2. Field sampling strategy

One of the key considerations in optimizing the antenna measurements is to design the sampling strategy which dictates at which spatial positions to measure the field strength for successful reconstruction of the radiation pattern. This mathematically translates to the problem of designing an $M \times N$ matrix where M is the number of measurements, N is the number of samples. Usually in compressed sensing, the practice is to acquire holographic measurements which is a linear combination of the coefficients. In this case, this is done by selecting specific rows (M rows) from the DFT matrix as the compressed sensing matrix.

Since compressed sensing is inherently different from interpolation technique it is ensure that the samples selected are well suited for recovering the signal. In other words, mathematically, the sampling matrix and the signal basis matrix must be maximally incoherent (mutual coherence of the CS matrix **A** must tend to the Welch bound). The performance of reconstruction depends on the mutual coherence properties of the CS matrix which in turn depends on the sensing/measurement matrix for a given sparsifying basis (chosen to represent the radiation pattern).

The first step to designing the sensing matrix Φ is to construct an Nx1 binary vector **b** which has 1 at positions where the field is sampled and 0 otherwise. This can be mathematically described as

$$\sum_{i=1}^{N} \Phi_{j,i} = 1; \forall j \in [1, M] \tag{3.9}$$

One way of assessing the viability of a chosen sampling scheme is to compute the point spread function (PSF) of a given sampling vector/matrix is a useful measure of the mutual coherence present in the sequence and also gives information about the extent of aliasing or interference present in the recovered signal. Given a sampling vector, the PSF is given by 3.10.

$$\text{PSF} = \frac{1}{\sqrt{N}} \Psi \mathbf{b} \tag{3.10}$$

where Ψ = $\mathbf{U}_N$ which is the unitary DFT matrix (used as the transform basis in this work).
Ideally when the full grid of points is sampled according to Nyquist criterion, the PSF has a maximum at the first index and zero elsewhere. But since compressed sensing requires lesser measurements than Nyquist, the characteristics of the PSF depends on how the samples are acquired (grid sampling strategy).

When DFT is used as the transformation basis, an equispaced under sampling of the signal/field pattern will give rise to grating lobes in the PSF which will give rise to aliasing when the radiation pattern is recovered. This is due to the fact that the mutual coherence between the columns of **A** is high in the case of equiangular undersampling. Hence when DFT is used as the transform basis, a random selection of samples from the conventional sampling grid of the field results in a good reconstruction of the signal as it results in an RPFM with near-optimal recovery guarantees. An example of equiangular and random under sampling are provided through simulations in the Fig. 3.3, 3.4.

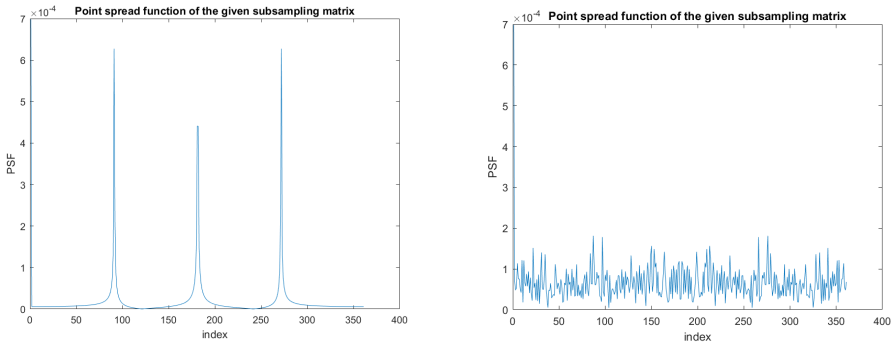

(a) Equiangular undersampled measurements

(b) Random undersampled measurements

Figure 3.3: Demonstration of presence and absence of aliasing in recovered signal for uniform and random undersampling of the pattern

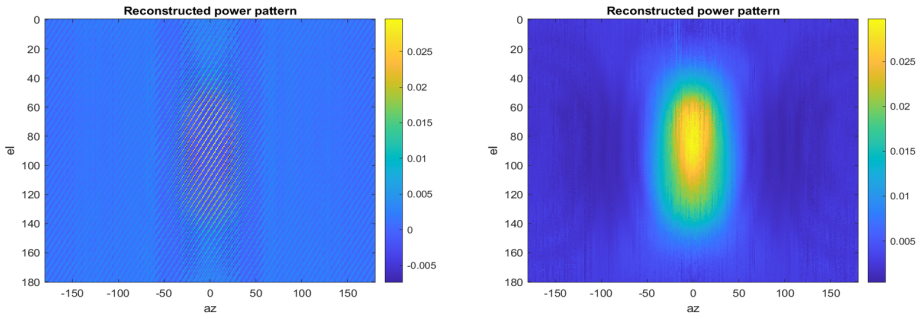

(a) Equiangular undersampled measurements **(b)** Random undersampled measurements

Figure 3.4: Demonstration of presence and absence of aliasing in recovered signal for uniform and random undersampling of the pattern

Figure 3.3 shows the grating lobes in the point spread function due equiangular measurements and the presence of the noise/interference floor in the presence of grating lobes. Its effects on the reconstruction of the 3D far-field radiation pattern of a pyramidal horn antenna is shown in Fig. 3.4.

However this is not the same case when the spherical harmonics are use to provide a sparse representation of the electric field. When spherical harmonic functions are used to compute the sparse coefficients to represent the radiation pattern, a minimum redundancy sampling technique can be followed. Certain optimal sampling methods have been proposed in literature in the context of spherical measurements. One of them that has been used in the work done in this thesis is the igloo sampling scheme which adaptively changes the sampling interval in the azimuth for a given elevation angular step. Say if $\Delta\theta$ is the sampling step in the elevation direction, the step size in the azimuth direction is given by

$$\Delta\phi = \frac{\Delta\theta}{cos\theta} \tag{3.11}$$

This reduces the number of samples compared to an equiangular grid yet still results in oversampling in the regions near the poles. Samples can be chosen in random from the grid of samples for a given $\Delta\theta$ in the igloo sampling method to estimate the underlying spherical wave coefficients and consequentially reconstruct the radiation pattern.

3.3. Performance metrics for evaluation

The standard performance metric used for the evaluation of the reconstructed signal in a compresseed sensing framework is the mean squared error (MSE) or the root-mean squared error (RMSE).

Given a far-field pattern/data $\mathbf{f}_n$ which is the field data to be measured (ground truth) and a recovered pattern $\hat{\mathbf{f}}_n$, the RMSE between them is

$$RMSE = \sqrt{\frac{1}{N}\sum_{n=1}^{N}\left(\mathbf{f}_n - \hat{\mathbf{f}}_n\right)^2} \tag{3.12}$$

Another potential error is the fractional error between the patterns and is defined as

$$f(L) = \sqrt{\frac{\sum_{\hat{\mathbf{r}}}\left|\mathbf{E}_{r,L}(\hat{\mathbf{r}}) - \mathbf{E}(\hat{\mathbf{r}})\right|^2}{\sum_{\hat{\mathbf{r}}}\left|\mathbf{E}(\hat{\mathbf{r}})\right|^2}} \tag{3.13}$$

There are several other metrics of error in literature as well which provide information about error in specific aspects of the radiation pattern [45].

Few of the metrics are the linear difference 3.14, weighted linear difference 3.15, logarithmic difference 3.16 and the weighted logarithmic difference 3.17.

$$\Delta_{lin}(\theta,\phi) = f_1(\theta,\phi) - f_2(\theta,\phi) \tag{3.14}$$

$$\Delta_{w,lin}(\theta,\phi) = W_{lin}\Delta_{lin}(\theta,\phi) \tag{3.15}$$

$$\Delta_{\log}(\theta,\phi) = 20\log_{10} f_1(\theta,\phi) - 20\log_{10} f_2(\theta,\phi) \tag{3.16}$$

$$\Delta_{w,\log}(\theta,\phi) = W_{\log}\Delta_{\log}(\theta,\phi) \tag{3.17}$$

where the weights can be formulated as $W_{log} = (f_1(\theta,\phi))^{\beta}$ where β can be chosen freely to an extent. This metric of error shows an increase in the relative level of error in the main lobe region which may be a useful performance metric when the goal is to ensure accuracy in the main lobe region rather than other aspects of the radiation pattern such as accuracy in side lobes or null depth.

In order to demonstrate the error parameters, the azimuth pattern of a horn antenna simulated using MATLAB is considered. The plot shows the simuated field pattern, the samples chosen as measurements and the recovered pattern. It can be observed from 3.5 that there are certain deviations between the simulated and recovered pattern have a considerable deviation at certain angular positions in the main lobe region (eg. difference at -24^o). Certain deviations are also observed in the side lobe region (eg. difference at 136^o as shown in 3.5).

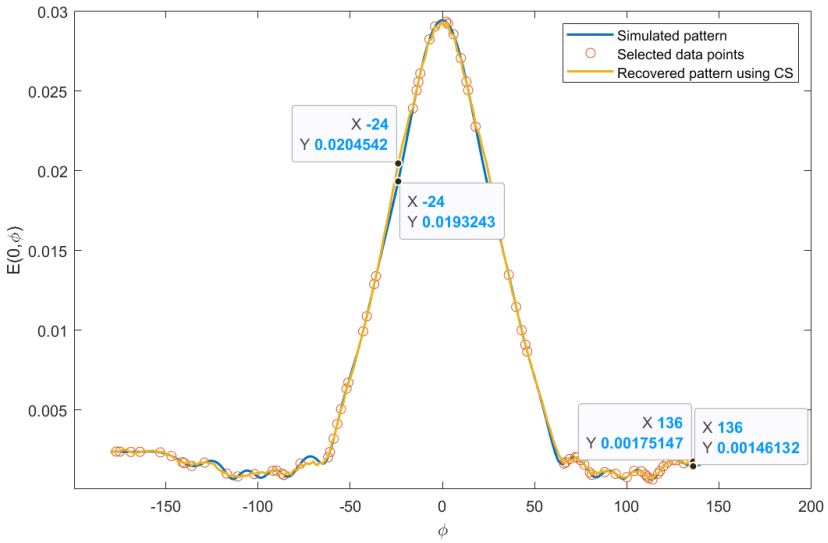

Figure 3.5: E-field patterns to be compared

A few other error metrics were defined in 2.2.4 which emphasize on different aspects of the radiation pattern.

The introduced error metrics are computed for the simulated and recovered antenna patterns and the results are shown in 3.6. Inferring from the results, it can be noted that weighted logarithmic difference emphasizes difference in the high power/main lobe region of the antenna radiation pattern giving less weights to the sidelobe regions. Linear difference (point wise) also provides a similar plot with higher variations in the main lobe region. From Fig.3.6, weighted linear difference (bottom left) and logarithmic difference (top right) shows variation in side-lobe regions where the power is comparitively lesser with more emphasis than the main lobe region. This demonstrates the use of different functions to compare the simulated and recovered pattern based on the required characteristic of the radiation pattern.

The mean and standard deviations of the differences between the ground truth and recovered patterns (linear or logarithmic) are useful error metrics. In addition to this, the errors can also be estab-

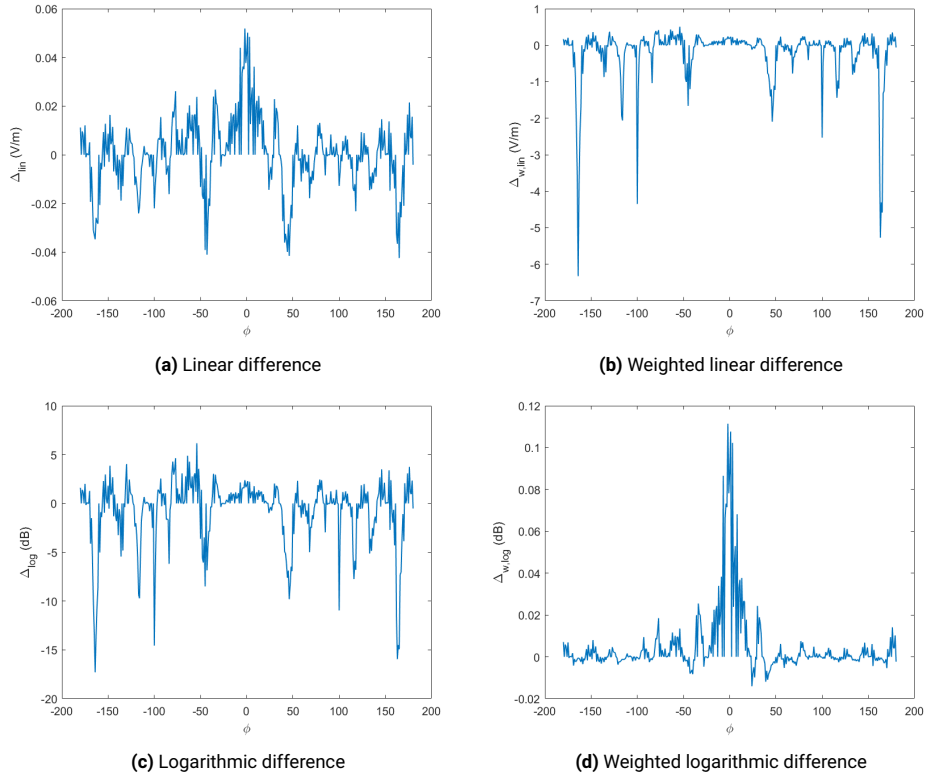

(a) Linear difference

(b) Weighted linear difference

(c) Logarithmic difference

(d) Weighted logarithmic difference

Figure 3.6: Various error metrics to compare radiation patterns

lished in terms of the simulated pattern which is expected according to the design and the recovered pattern by extracting specific parameters from them. In this work, the error in the following parameters are of concern:

1. Maximum Gain (G_0) or Directivity (D_0)
2. Half-power beamwidth (HPBW)
3. Peak sidelobe level (PSLL)
4. Average sidelobe level (ASLL)

3.4. Modeling non-idealities in antenna radiation patterns

Fabrication and operation error modeling: The weighted l_1 minimization procedure uses prior information from electromagnetic simulation of the AUT to find the underlying coefficients according to the sparsity transform and use the obtained coefficients to formulate the weights for the algorithm. But it is critical to ensure that the assignment of weights from prior information does not result in loss of information of the ground truth (true radiation characteristics of the AUT). It is important to ensure the same as we need to be able to measure the deviations of the measured pattern from the ideal to understand whether there are manufacturing discrepancies or unknown effects in the design causing deviation of the pattern from the expected simulation results. For this reason, in this work, errors have been introduced to distort the ideal radiation pattern in simulations to compare the recovered pattern with both the simulated and distorted pattern. This is used to know if the reconstruction is closer to the measured pattern or the simulated pattern and if the recovery performs well, the result must have a smaller value of error in comparison with the measured pattern.

In single element antennas, the errors may arise due to manufacturing defects and errors in dimensions of the radiating structure etc. In terms of antenna arrays, there is a wider range of possible errors [46]. Mutual coupling arises due to the coupling between the array elements and it creates undesirable distortions in the pattern which result in variation in the sidelobe levels of the resulting array patterns.

Due to the presence of mutual coupling, the embedded element patterns of each element in the array may vary significantly [12]. Errors in element positions, amplitude and phase excitations are also very much possible and it is necessary to be able to measure these effects during the CS based sampling and recovery. Apart from errors in the pattern, the methods must also work in scenarios where the main beam of an array is scanned to a specific direction and measure the true radiation pattern of the AUT for these scenarios.

For the work done in this thesis, to verify the performance of the recovery methods on patterns with measurement noise, Some of the effects considered during testing of the pattern reconstruction in the work done are

1. Scanning main beam to target direction
2. Mutual coupling effects (in arrays)
3. Reduced beam width

3.5. Conclusions

This chapter discussed the signal model that dictates the application of compressed sensing to reducing the number of samples for antenna pattern measurements. The benchmark method (l_1-norm), new method (weighted l_1-norm minimization) and another method of using re-weighted l_1-norm minimization. The workflow of the pipeline is explained. The section on field sampling strategy discusses the properties of CS that must satisfied to enable exact recovery of the signal (pattern in this case).

4

Sparse recovery using compressed sensing

4.1. Sparsity in radiation patterns

4.1.1. Transform basis: DFT

In order to recover the pattern from a sparse set of measurements using compressed sensing, it is necessary to first demonstrate the sparsity of antenna radiation patterns in the Fourier domain (DFT) cite equation. In order to compute an approximate value of the sparsity, the signal coefficients $\mathbf{x}_{sim}$ which cross a threshold have been considered and the support of the result is taken as the sparsity present in the signal. The comparison of the number of samples and the support of the coefficients vector (sparse) is shown in the table 4.1 for both 2D pattern cuts and 3D radiation data.

Table 4.1: Sparsity levels of different radiation patterns

Antenna	Pattern type	Number of grid points (N)	Number of sparse coefficients(K)	Sparsity (K/N)
Pyramidal Horn	1D (E-plane)	361	37	10.2%
4-element patch array	1D (H-plane)	361	75	20.78%
Pyramidal Horn	3D	65534	5534	8.5%
Cassegrain antenna	3D	16471	513	4%
Dipole	3D	16471	160	1%
Helix antenna	3D	16471	310	2%
Vivaldi	3D	16471	1523	9.25%

It can be inferred from the above table that a wide range of antenna patterns provide a sparse representation in transform domain using the DFT basis. The sparsity in the radiation patterns enables the use of compressive sampling and reconstruction from reduced number of measurements, which is related to the sparsity/compressibility of the signal. If the sparsity value K is less, the pattern can be recovered using lesser measurements and this relation is demonstrated in the following sections. Another visualization of the sparse DFT coefficients for the azimuth pattern cut and the three-dimensional radiation pattern data of a pyramidal horn antenna operating at 7.67GHz is shown in the figure 4.1.

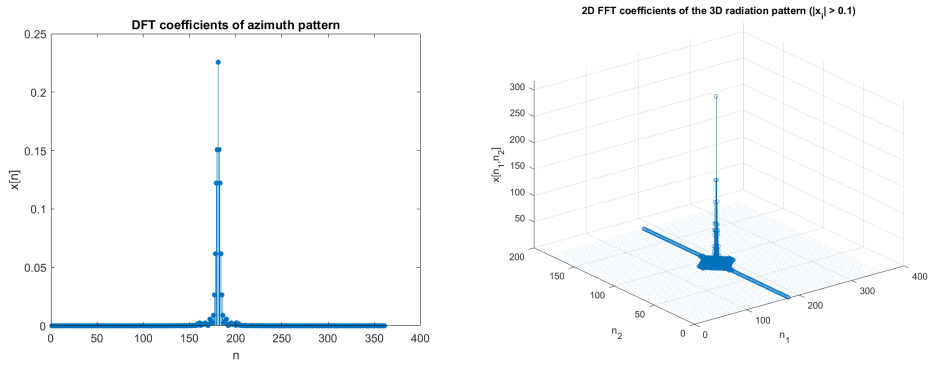

(a) Coefficients of Azimuth pattern (2D)

(b) Coefficients of 3D pattern

Figure 4.1: DFT coefficients for pattern of a pyramidal horn antenna

4.1.2. Transform basis: Spherical harmonics

The electric field radiation pattern of any AUT can be expressed in terms of a linear combination of spherical harmonics of degree l, order m (Eqn. 2.12). During the computation, the infinite summation is reduced to a finite sum by a truncation order L which depends on the frequency of operation and the maximum dimension of the antenna. The spherical wave coefficients that are used in the expansion to represent the electric field is sparse for most antennas considered. This motivates the use of a redundant sampling scheme and compressed sensing techniques to recover the field pattern from lesser number of measurements. In this chapter, first the sparse nature of the spherical wave coefficients is demonstrated for the radiation patterns considered using the spherical mode spectrum of the radiated fields. Later, the igloo sampling scheme is used to select redundant number of samples for recovery using l_1 norm minimization. Further, a subset of samples from the igloo sampling grid are chosen and used for recovery of the radiation pattern and in this, the performance of both l_1 as well as weighted l_1 norm minimization techniques are compared to select the best recovery algorithm.

An overview of the antennas considered during simulations as well as its maximum dimensions, corresponding truncation order L and number of samples used to recover the field pattern with good accuracy are shown in the table 4.2. As mentioned in chapter 2, the truncation order is computed as $[\frac{2\pi a}{\lambda}] + n_1$ where $n_1 = 10$ typically. L is dependent on the frequency of operation as well as the physical size of the radiating structure.

Table 4.2: Sparsity levels of different radiation patterns

Antenna	Frequency (GHz)	$\frac{2\pi a}{\lambda}$	L	N = $(L+1)^2$	M_{igloo}
Vivaldi antenna	3.5	18	30	961	961
Pyramidal horn	7.87	17	30	961	961
Sparse array (64 elements)	25.75	32	50	2601	2594
Patch array (4 elements)	5	28	50	2601	2594

Given a truncation order L, there are $N = (L+1)^2$ spherical wave coefficients to represent the electric field and for accurate estimation of the coefficients, conventionally $M \approx N$ measurements are required. For good recovery, the M measurements are selected from the redundant igloo sampling scheme where the angular step in the elevation ($\Delta\theta$) is fixed and the step in azimuth ($\Delta\phi$) is computed at each θ. If the recommended sampling grid has an equiangular step size of 1^o, the field over the dense grid can be estimated from estimate of the coefficients using compressed sensing and retrieving the field with the known spherical harmonic functions.

4.2. Reconstruction using l_1 and weighted l_1-norm minimization

4.2.1. Transform basis: DFT

Currently employed methods for antenna measurements using compressed sensing use l_1-norm minimization as the method to estimate the underlying sparse coefficients of the field and consequentially the radiation pattern data is recovered. Hence, the conventional basis pursuit is chosen as the benchmark for comparing the proposed recovery method and the weighted l_1 method is compared with it.

In this work, the idea is to use prior information available on the AUT from simulations to optimize the measurements. This can be done by designing weighting functions using the available knowledge of the sparse coefficients from electromagnetic simulations of the antenna's radiation characteristics. The computed weights for a given set of simulated coefficients from the azimuth pattern ($\theta = 0$) of a pyramidal horn antenna is given in the figure 4.2. The designed weight function can be used in the modified optimization problem (thereby enhancing sparsity in the data). The major advantage of using weighted l_1 norm minimization is the significant reduction in the required number of measurements as compared to the l_1 norm based approach for a desired accuracy. Reducing the number of measurements enables faster characterization of the AUT which is desired in antenna measurements. However, to use the method with certainty, it is also critical to investigate the estimation of coefficients in regions outside the support of the simulated coefficients. In order to compare the performance, both l_1 and weighted l_1 minimization based recovery is performed on various antenna patterns.

In the first case, a standard pyramidal horn antenna (operating at a frequency of 7.87GHz) is simulated using the Antenna Toolbox in MATLAB. The azimuth pattern of the antenna is chosen with a sampling of $\Delta\theta = 1^o$.

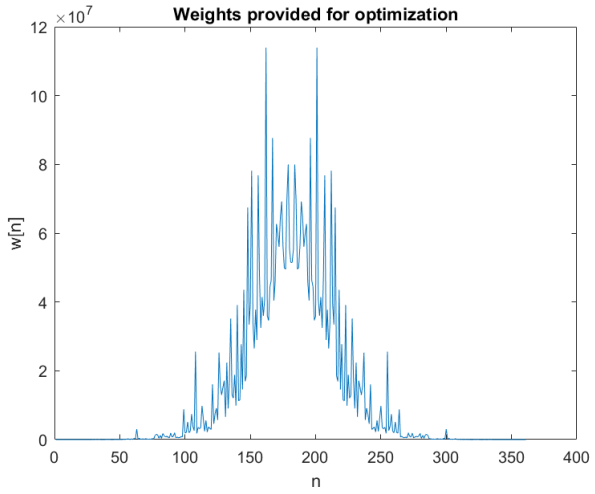

Figure 4.2: Weight function computed as the inverse of coefficients obtained from simulated pattern

Figure 4.2 gives an idea of the magnitude of weights (inverse of coefficients) provided in the cost function of the optimization problem. The value of weights is higher for coefficients with small amplitude and vice versa for larger magnitude coefficients. The performance of recovery from 30 (out of 360) measurements, using l_1-norm and weighted l_1-norm minimization problems are shown in Fig. 4.3.

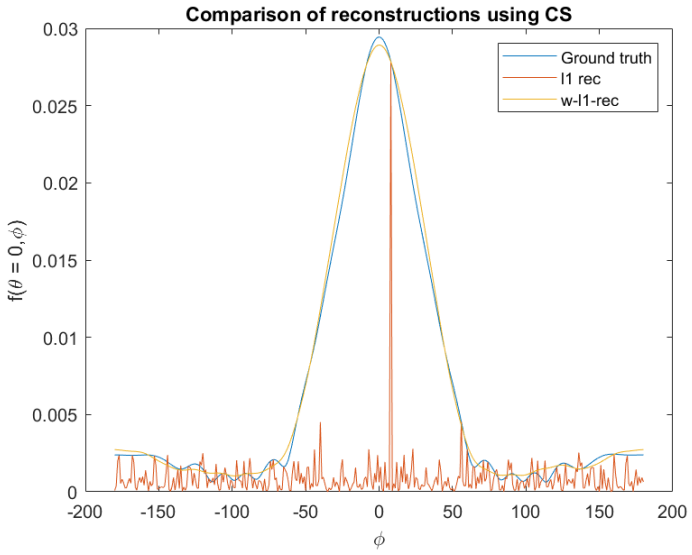

Figure 4.3: Comparing recovery of l_1 to weighted l_1 norm minimization (M = N/12)

The estimated coefficients using both algorithms which then undergo the transform to give the estimates of the field patterns are shown in the Fig. 4.4.

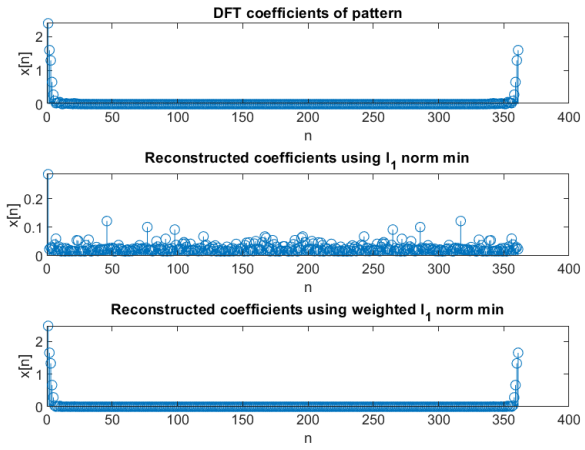

Figure 4.4: Coefficients estimated from l_1 and weighted l_1 minimization

It can be seen from fig. 4.3 that the weighted l_1 minimization provides a much better recovery of the underlying sparse DFT coefficients of the radiation pattern compared to the l_1 minimization used in basis pursuit compressed sensing. This is due to the high value of weights (shown in Fig. 4.2 assigned to low valued coefficients in the sparse vector which brings the minimization closer to l_0 norm minimization that is ideally required to estimate the coefficients.

The performance of the recovery is assessed by computing the root mean squared error between the simulated and recovered patterns. It can be inferred from fig.4.5 that weighted l_1 algorithm performs much better for less number of measurements and the idea is that if a RMSE of 3 $(V/m)^2$ is the accuracy required for faithful reconstruction, this can be achieved using just 15% of the total number of samples as opposed to 30% measurements required using l_1 based recovery.

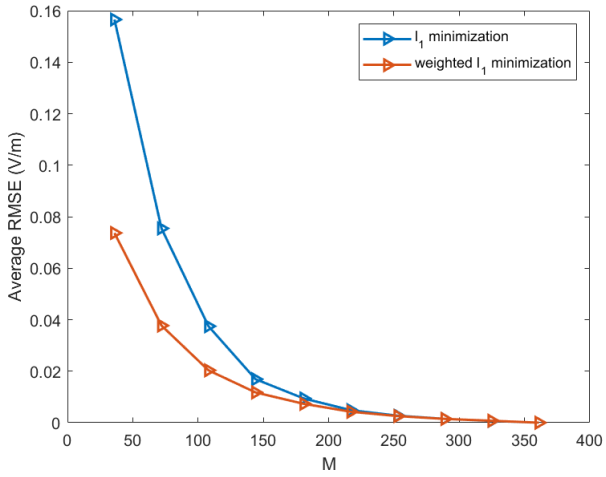

Figure 4.5: RMSE as a function of number of measurements for azimuth pattern form pyramidal horn antenna

The below set of figures demonstrate the recovery of a 3D antenna radiation pattern shown as an equirectangular projection. The far-field radiation pattern of a Vivaldi antenna operating at 3.5GHz has been simulated and it is shown in fig.4.6a.

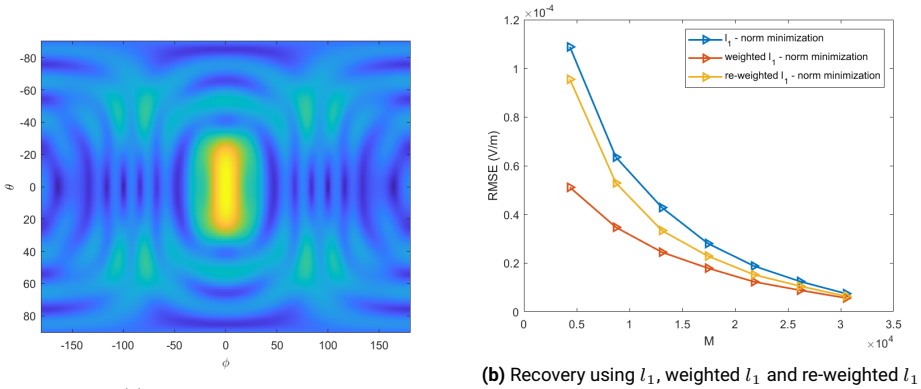

(a) 3D radiation pattern

(b) Recovery using l_1, weighted l_1 and re-weighted l_1 minimization

Figure 4.6: Compressed sensing based sampling and reconstruction of Vivaldi antenna paatterns

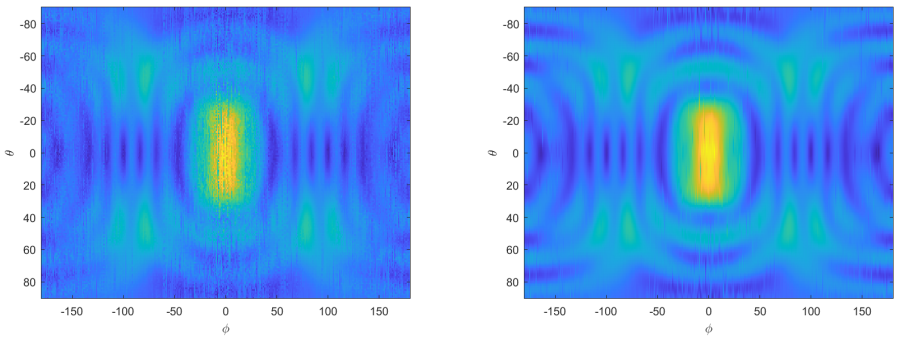

(a) Recovery using l_1 minimization

(b) Recovery using weighted l_1 minimization

Figure 4.7: Compressed sensing based sampling and reconstruction of Vivaldi antenna patterns (M = 13000)

Fig. 4.6 shows the RMSE vs M plot for all three reconstruction methods mentioned in the signal model and the weighted l_1-based recovery is much better than both re-weighted l_1 or l_1- norm mini-

mization. For this reason, all analysis and discussions that follow further in the report, are comparing l_1 with weighted l_1-minimization based results.

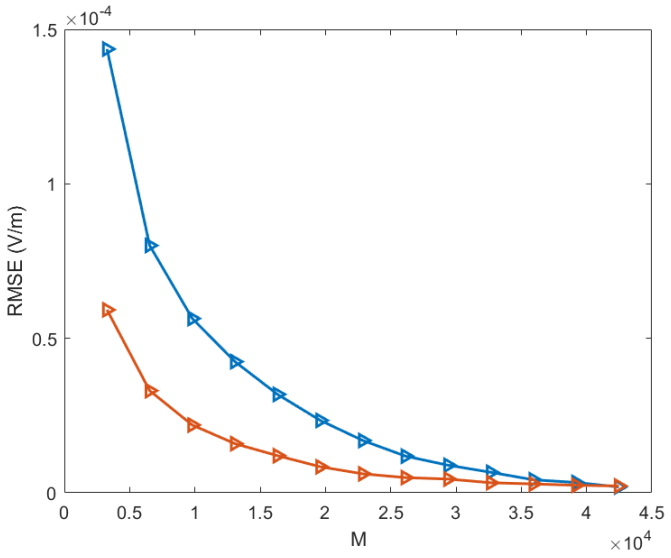

Figure 4.8: Recovery using l_1 minimization

The patterns are recovered using both algorithms from M = 13000 measurements (M/N=20%) and the results are shown in fig. 4.7. It is evident from comparing the recoveries that weighted l_1 norm recovery performs much better than the benchmark as the recovery using l_1 minimization has a lot of gaps in the data reconstructing which manifest as undesirable artifacts in the radiation pattern which distort the resulting pattern. The M samples used to reconstruct the field pattern are chosen uniformly at random from the regular grid of field points as this results in less coherence of the measurement matrix **A**.

4.2.2. Transform basis: Spherical Harmonics

In this section, the results from reconstruction of radiation pattern of three antennas from a reduced set of samples using compressed sensing methods is presented. The antennas considered are a sparse 2D array of patch elements, a 4 element patch array and Vivaldi antenna. The results corresponding to each antenna are presented as follows:

Vivaldi antenna

To provide a fair comparison between recovery while using both the bases functions, the Vivaldi antenna (operating at 3.5GHz) data that has been used previously in the DFT basis has been used to recover the data. The spherical mode expansion of the electric field (fig. 4.6a) of the Vivaldi element is shown in Fig. 4.9a. It can be observed that since the sparsity is high in the spherical wave coefficients, i.e. there are only very few non-zero coefficients, there is not a very significant improvement in using weighted l_1-method over the l_1 method in terms of the reduction in number of field samples required. The RMSE plot is obtained by performing a Monte Carlo analysis of 10 iterations, since samples are chosen at random from the igloo sampling grid. The number of samples/measurements vary from 100 to 2000.

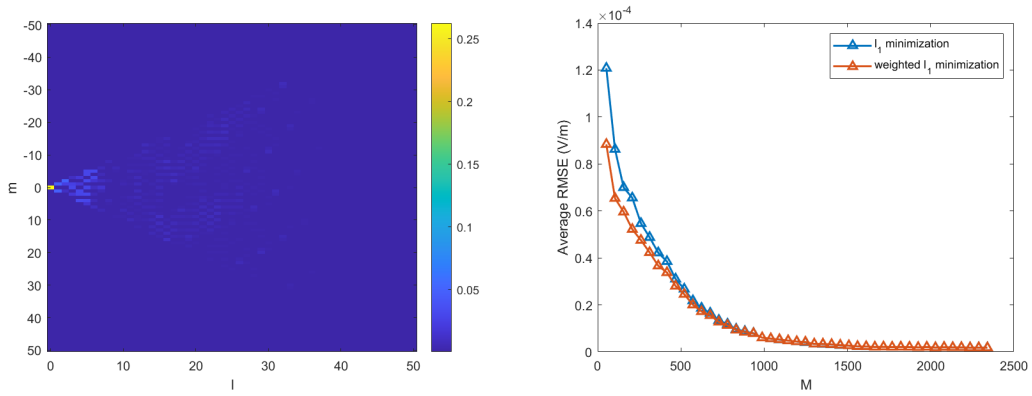

(a) Spherical mode coefficients **(b)** RMSE vs number of measurements plot

Figure 4.9: Vivaldi antenna

Patch array

Another example demonstrating the effectiveness of spherical harmonic expansion in recovering the field and the capability of weighted l_1-norm minimization to provide better accuracy for lesser number of samples is shown. The data from simulations of a 4-element patch array (operating at 5GHz) has been used for analysis. Fig. 4.10 shows the simulated pattern and the pattern when reconstructed using the benchmark l_1-minimization from 2594 samples in the Igloo sampling grid. The performance of both methods (l_1 and weighted l_1) is shown in Fig. 4.11 along with its spherical mode coefficients.

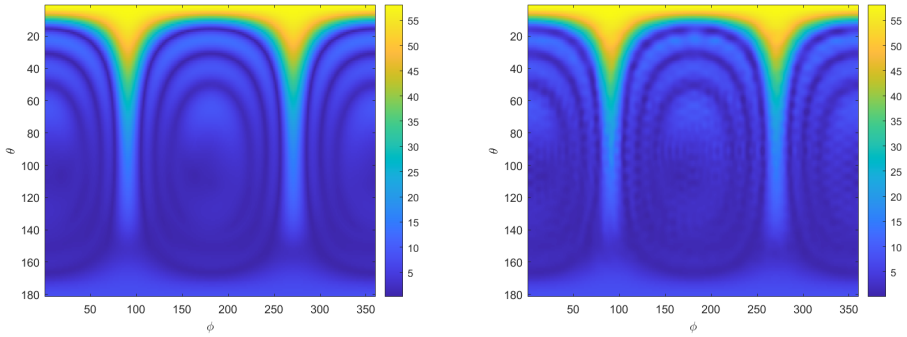

(a) Simulated patch array pattern **(b)** Pattern recovery from 2594 samples from Igloo grid

Figure 4.10: Compressed sensing based sampling and reconstruction of the 3D patterns of pyramidal horn

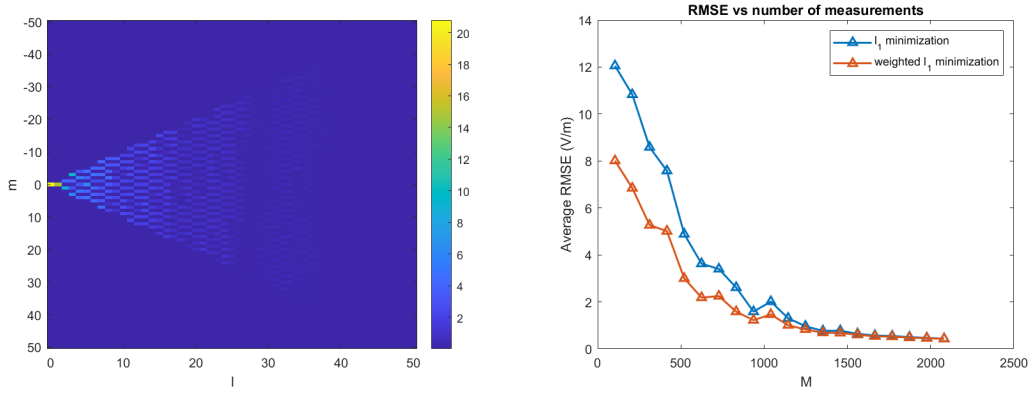

(a) Spherical mode coefficients **(b)** RMSE vs number of measurements plot

Figure 4.11: Patch array with 4 radiating elements

Sparse 2D array

In this section, a 2D sparse array (of patch elements) operating at 25.75GHz frequency, designed and tested at the Microwave Sensing, Signals and Systems (MS3) group at TU Delft has been considered. The array consists of 64 patch antennas and its radiation pattern (equirectangular) and spherical wave coefficients are shown in Fig. 4.12.

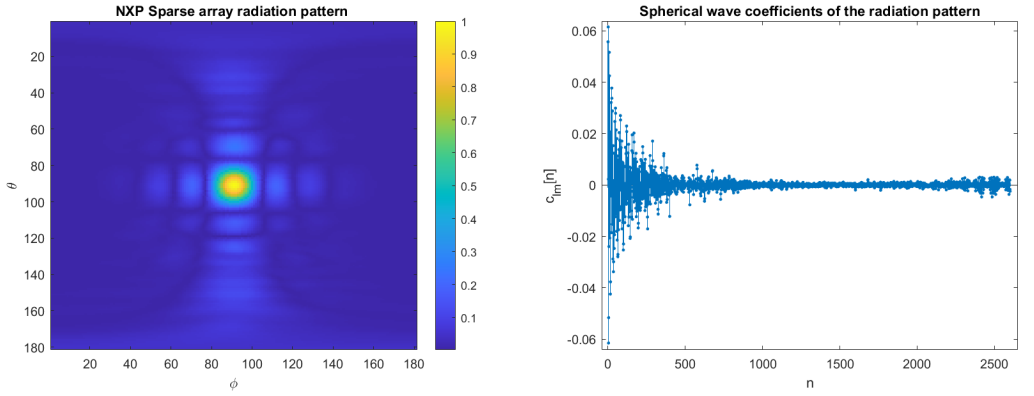

(a) Equi rectangular pattern of the AUT considered

(b) N spherical wave coefficients of the radiation pattern

Figure 4.12: Radiation pattern of NXP sparse array measured at DUCAT (MS3)

The spherical wave coefficients c_{lm} can also be grouped based on their degree and order to represent the mode spectrum of the field which gives insights into the most prominent modes of spherical harmonics that contribute to the radiated field. The mode spectrum of the sparse array considered is shown in Fig. 4.14a. It can be observed that of the 2601 coefficients computed (for L=50), only a small fraction of coefficients (having lower degree) are significant, thereby demonstrating the underlying sparsity in the data.

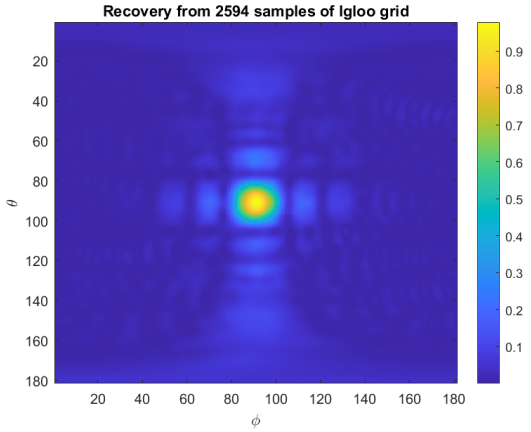

Figure 4.13: Pattern recovered using weighted l_1 minimization with the entire igloo sampling grid

Once again, as discussed in the case of the DFT based reconstruction, the recovery has been attempted for various number of measurements by solving both the l_1 and weighted l_1 norm minimization problems in order to analyze which performs better. The number of samples measured/chosen for reconstruction (denoted by M) is varied from 100 samples upto 2000 samples and the root mean squared error between the ground truth and the reconstructed pattern is used as a performance metric. The field measurements are chosen in random from the igloo sampling grid as random sampling has near-optimal recovery guarantees in compressed sensing using spherical harmonics. The weights for the weighted l_1-norm minimization are constructed using the prior knowledge of the field from simulations. An example of the recovered pattern using all the grid points in the igloo sampling grid has been

shown in Fig. 4.13

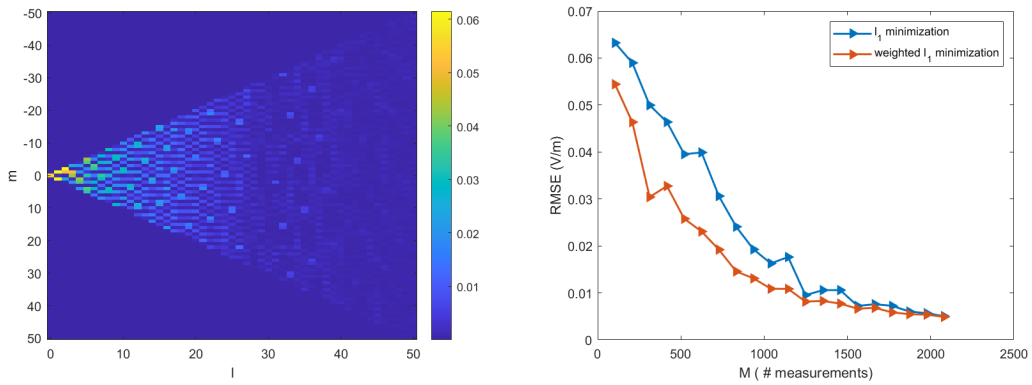

(a) Spherical mode coefficients

(b) RMSE vs number of measurements plot

Figure 4.14: Results for the compressed sensing for sparse array pattern recovery

The RMSE plotted for each number of measurements considered (M) is the average error value from 10 different set of samples chosen at random. The RMSE curve for recovery using weighted l_1-norm minimization lies below the curve corresponding to l_1-norm minimization (chosen benchmark) which demonstrates that there is an evident reduction in the number of samples required to reconstruct the radiation pattern for a specified RMSE value. For example, it is possible to achieve an RMSE error as low as 22.7 mV/m with 520 samples using the new method as opposed to the existing benchmark recovery which required 840 samples.

4.2.3. Comparing basis functions

During the course of this thesis, the methods were investigated by representing antenna patterns using both DFT and spherical harmonic functions. Let us consider the weighted l_1-norm minimization which is proven to be a better recovery technique in the context of antenna measurements from earlier presented results. For a simple demonstration of both the sparsifying bases, the radiation patterns of Vivaldi and pyramidal horn antenna are reconstructed by representing the fields through both basis functions and the results are tabulated in the table 4.3.

Table 4.3: Sparsity levels of different radiation patterns

Antenna	N_{field}	M_{DFT}	M_{SHE}	$RMSE_{DFT}$	$RMSE_{SHE}$
Vivaldi antenna	65341	13069	936	2×10^{-4}	2×10^{-4}
Vivaldi antenna	65341	3269	156	6×10^{-4}	6×10^{-4}
Pyramidal horn	65341	13069	832	2.66×10^{-4}	2×10^{-4}

From the table 4.3, we can conclude that the spherical harmonics can recover the pattern with far lesser number of samples than compared to the DFT as the transform basis.

4.3. Reconstruction of non-ideal radiation patterns

Due to the design of the weights applied to the coefficients based on prior information from simulations, it is essential to validate the proper functioning of the proposed method (weighted l_1-norm minimization) on patterns that contain distortions and measurement noise. The method must also provide good reconstruction of the ground truth (field radiated by the AUT during measurement process) rather than creating bias. In simpler words, the recovered pattern must be close to the ground truth than to the simulated pattern. To ensure this fact, the weights are constructed by introducing a tolerance parameter ϵ which allows estimation of coefficients beyond the support of simulations.

The working of the proposed method on patterns with distortions or varying characteristics are demonstrated using the simulation of a 9-element half-wave dipole uniform linear array (ULA) designed using the antenna toolbox in MATLAB. The elements operate at their resonant frequency of 1.8GHz and the spacing between consecutive elements is 0.49λ in order to avoid effects of mutual coupling.

Two types of variations are introduced to the patterns in this work. The first one is scanning of the main beam to an angle of $\phi_s = 120^o$ from its initial design at $\phi = 90^o$. This is done by providing a progressive phase shift of $\beta = 124.7$ to the elements in the ULA. A drop in the peak of the main beam is observed according to cosine law. The pattern without the phase shifts is considered as the prior information available and it is required to measure the scanned beam pattern. Both the methods (l_1 and weighted l_1 minimization) are applied on 120 pattern samples (M=120, N=717) chosen in random to recover the azimuth pattern.

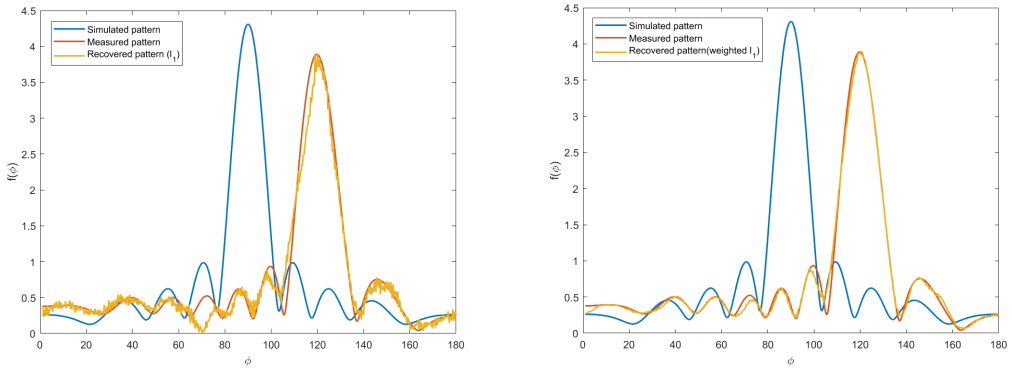

(a) Caption **(b)** Caption

Figure 4.15: Re-weighted l_1-norm recovery - reconstructed pattern and residuals plot

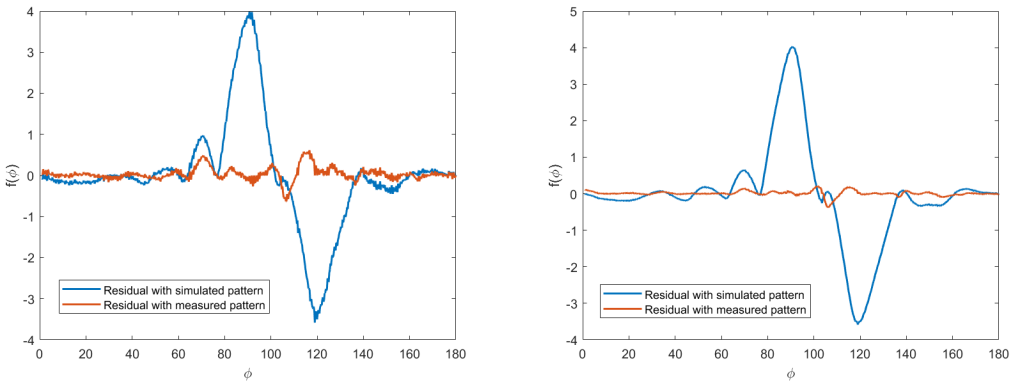

(a) Caption **(b)** Caption

Figure 4.16: Pattern distorted due to spacing between elements - recovery with (M=120, N=717)

Observing figures 4.15,4.16, the recovered pattern from both methods match more with the measurement (ground truth) than with the simulated prior information as expected. And it can also be noted that the magnitude of residual with measured pattern is less for the proposed method than with the benchmark.

The second variation considered is the reduction of beamwidth of the main lobe of the radiation pattern. This significantly distorts the antenna pattern and the distorted pattern is considered the ground truth to be reconstructed. It follows a similar inference as with the previous case, with weighted l_1 minimization performing better (lesser error in the residual).

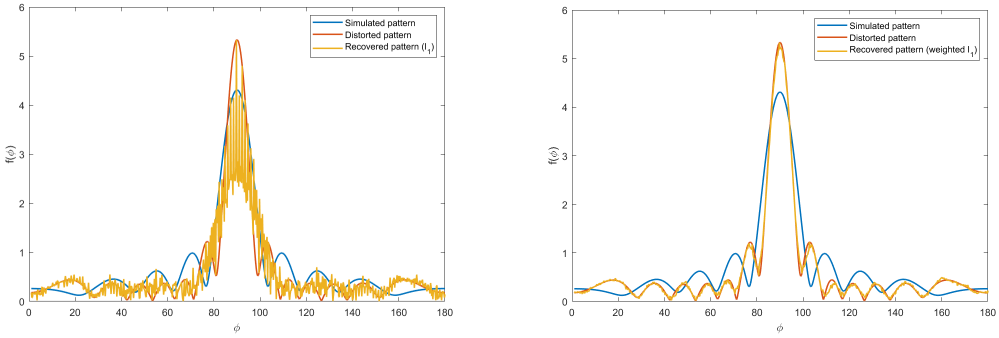

(a) Caption **(b)** Caption

Figure 4.17: Pattern distorted due to spacing between elements - recovery with (M=120, N=717)

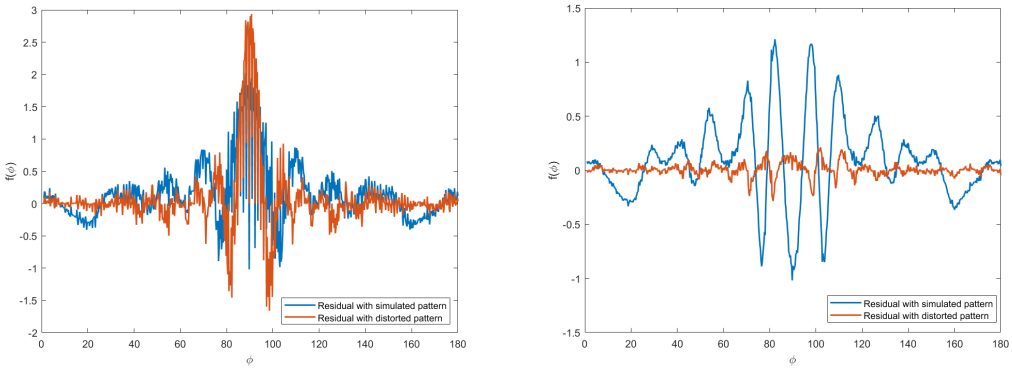

(a) Caption **(b)** Caption

Figure 4.18: Pattern distorted due to spacing between elements - recovery with (M=120, N=717)

4.3.1. Results from measurement data: Patch array of 4 elements

To further validate the applicability of the reconstruction method, the method has been tested on azimuth cut pattern data of a patch array operating at a frequency of 5GHz. The data used for testing the method was measured at the DUCAT chamber in the microwave sensing, signals and systems (MS3) group at TU Delft[1]. The expected radiation pattern is obtained using CST simulations of the patch array and is used as prior information to construct the weights and samples are chosen at random from the measured data. The simulated and measured patterns are shown in Fig. 4.19. It can be observed that the mutual coupling in the array and other measurement noise produce error in the side lobe regions of the pattern.

Fig. 4.20,4.21 show the recovered pattern (from 73 samples) using both l_1 and weighted l_1-norm minimization and their corresponding residuals with both the simulated and measured pattern. It can be observed that in both cases, the residual between recovered and measured patterns is lower than that between recovered and simulated, which is desired. It can further be noted that the magnitude of error is much higher in the pattern reconstructed from weighted l_1 minimization rather than the l_1 minimization which demonstrates its better performance compared to the existing benchmark technique.

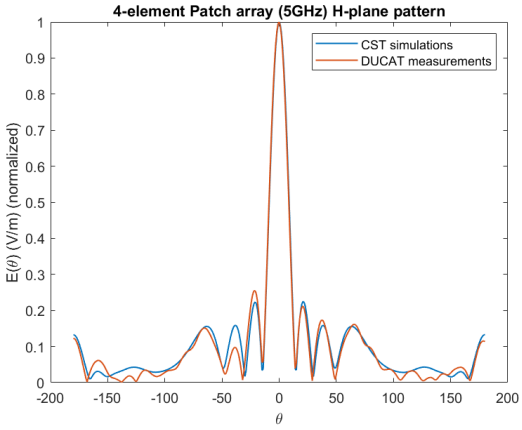

Figure 4.19: Simulated and measured patch array H-plane pattern

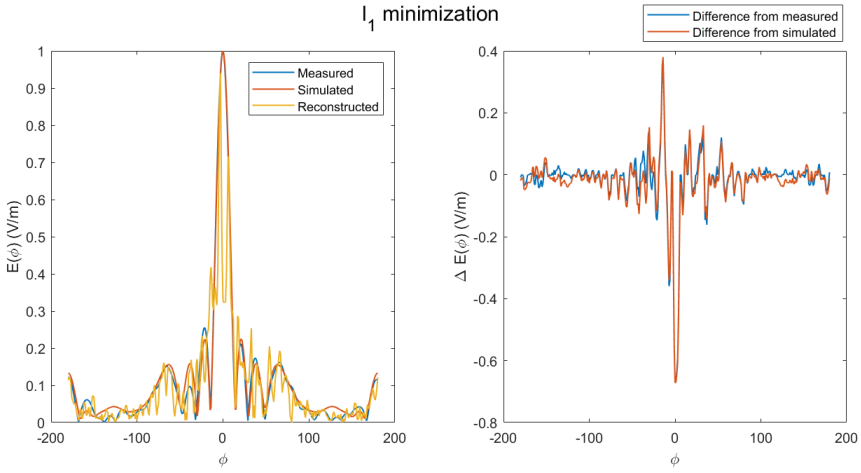

Figure 4.20: Recovered pattern using l_1 minimization and error when compared with simulated and measured pattern

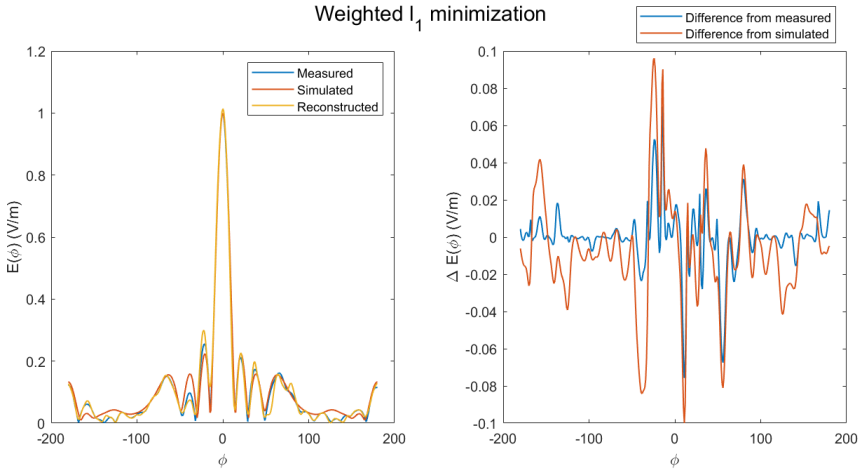

Figure 4.21: Recovered pattern using weighted l_1 minimization and error when compared with simulated and measured pattern

4.4. Conclusions

From the results in this chapter, the spherical harmonic basis provides a sparse representation of the radiation pattern allowing the electric field to be represented with few non-zero coefficients. This enables a great reduction in the number of samples required to recover the pattern information when compared to using the DFT as the transform basis. The difference observed between the two is that, spherical harmonics requires selection of measurements in random from the set of sampling locations in an igloo field sampling grid. Whereas, in case of the DFT, the selection of sampling locations is completely random to reduce the mutual coherence between DFT basis matrix and the sub-sampling matrix. The random partial Fourier matrices constructed in this manner are near-optimal CS matrices.

For both the set of basis functions, the patterns have been recovered by solving both the l_1 and weighted l_1-norm minimization problems and it can be concluded that the new method (weighted l_1) provides better results (reduced number of samples for given accuracy) but the extent to which the method performs better than the existing benchmark depends on the sparsity levels of the considered radiation pattern.

Various non-idealities in the radiation pattern was studied to make sure the new method is able to recover the distorted patterns with good accuracy.

5

Performance of recovery under different error metrics

5.1. Error metrics comparison

For the pyramidal horn antenna (azimuth pattern), the error parameters (defined in previous section) are computed as a group of box plots for given number of samples. Each box plot contains about 1000 error values from a Monte Carlo analysis.The box plots give a graphical demonstration of the spread of numeric data by splitting the data points based on their values into quartiles. The size of the box plot represent the distribution/dispersion of the values of data points considered. In this case, the box plots represent the various error parameters that are computed between the simulated radiation pattern which is used as the reference and the recovered pattern using compressed sensing.

The analysis has been done for different error parameters by considering 1000 random sampling configurations to acquire data for a given number of samples M. The sampling ratio (M/N) is considered to vary from 10% to 90% in steps of 10% to perform the analysis.

M/N = [10%, 20%, 30%, 40%, 50%, 60%, 70%, 80%, 90%]

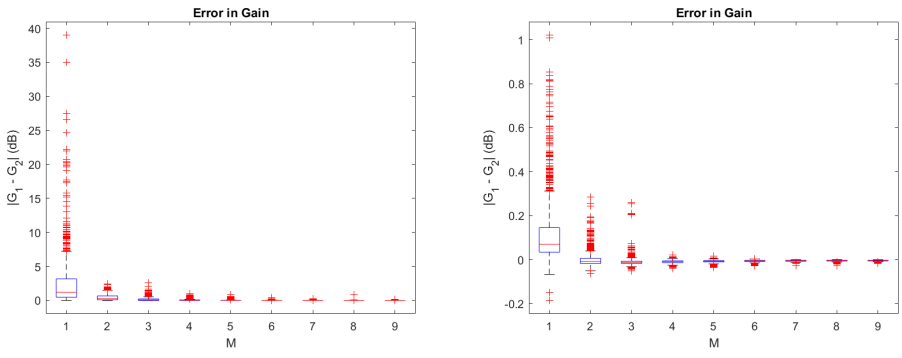

(a) Recovery using l_1 minimization

(b) Recovery using weighted l_1 minimization

Figure 5.1: Box plots showing error in Gain

It can be observed that the size of the box plots and the number of outliers beyond the whiskers of each box plot reduces with increasing number of measurements. This validates the logic that the probability of exact recovery increases with increasing number of measurements of the field. It is also to

be noted that despite the number of measurements, certain sampling vectors (configurations) provide a better recovery corresponding to the considered error pattern.

But the most important implication from this type of analysis is that when the number of radiation pattern samples are in the lower end (10-40%), it can be clearly observed that the errors in patterns recovered using weighted l_1-norm minimization is much smaller when compared to the recovery using the benchmark.When considering gain, the peak error for patterns recovered using 10% samples in l_1-minimization is almost 7dB whereas that corresponding to weighted l_1-minimization is only 0.3dB which is a significant improvement in recovery.

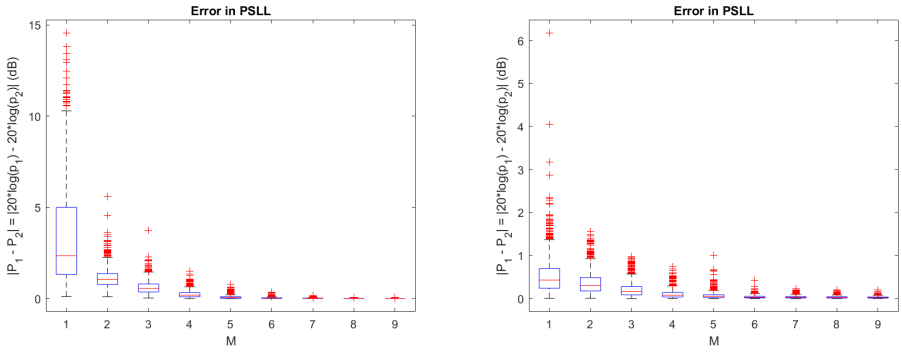

(a) Recovery using l_1 minimization **(b)** Recovery using weighted l_1 minimization

Figure 5.2: Box plots showing error in peak side lobe level (PSLL)

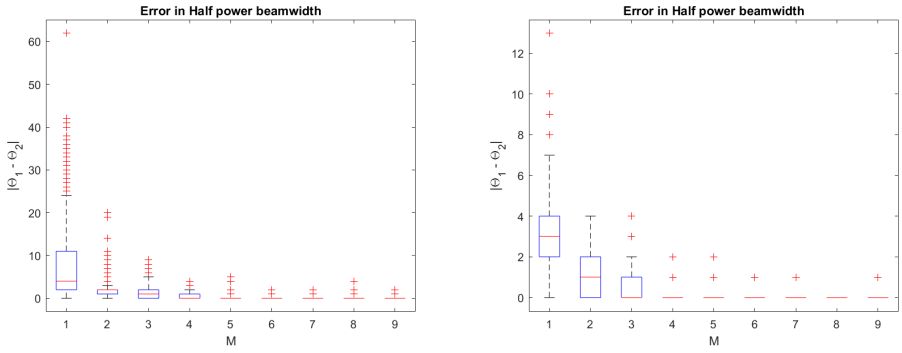

(a) Recovery using l_1 minimization **(b)** Recovery using weighted l_1 minimization

Figure 5.3: Box plots showing error in half power beamwidth (HPBW)

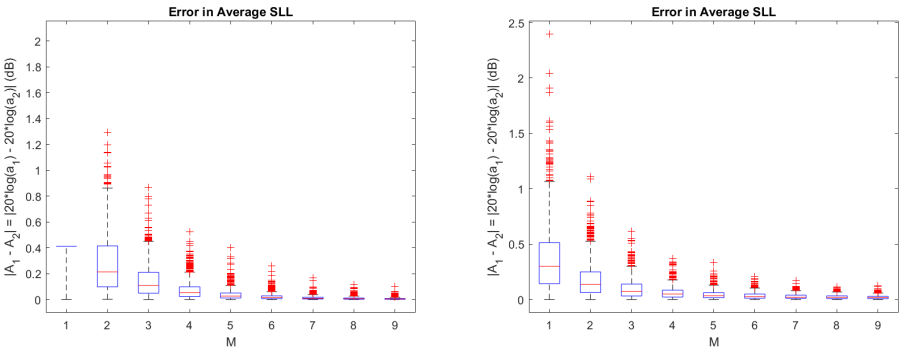

(a) Recovery using l_1 minimization **(b)** Recovery using weighted l_1 minimization

Figure 5.4: Box plots showing error in average side lobe level (ASLL)

5.2. Selection of sub-optimal sampling grids

Despite the fact that a minimum number of samples guarantees a high probability of exact recovery, it can be observed from the boxplots that there are certain random sampling vectors that provide near-optimal recovery of the considered error quantity. There are certain error values on the lower bound of the box plots that a minimum value of the error quantity considered can be achieved by a specific ideal configuration of samples which results in a sub optimal sampling strategy for a given number of samples to measure.

The simulation has been performed on the azimuth pattern of a Vivaldi antenna (consisting of 361 samples) operating at 5GHz. The set of samples that result in minimum error in gain, half power beam width and peak side lobe level have been identified from a Monte Carlo simulation of 1000 iterations and each of the error metric has been computed for the sampling scheme.

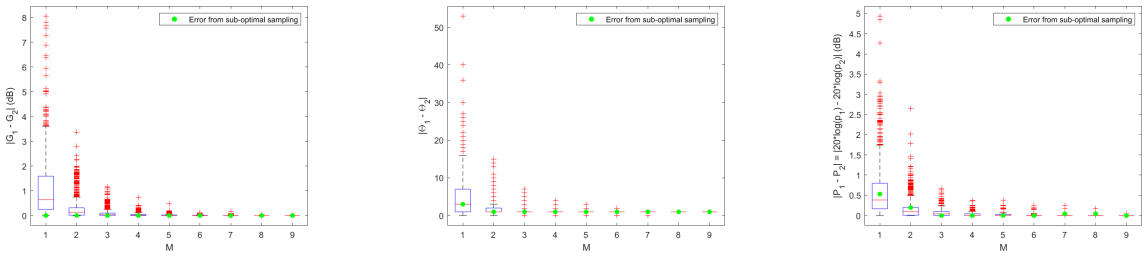

(a) Error in Gain (dB) **(b)** Error in HPBW **(c)** Error in PSLL (dB)

Figure 5.5: Sampling vector resulting in minimum error in Gain chosen for each number of measurements M

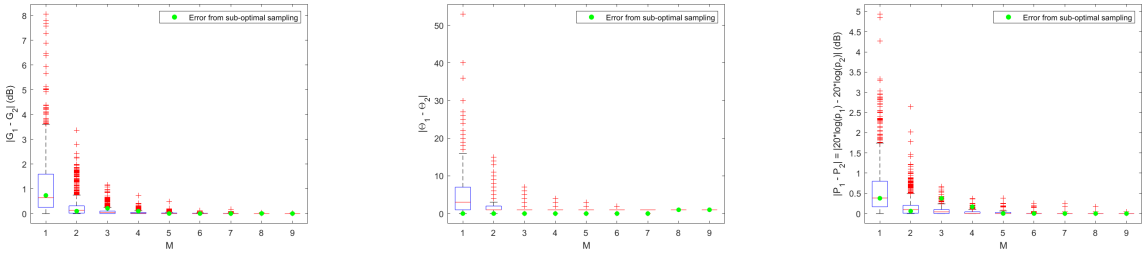

(a) Error in Gain (dB) **(b)** Error in HPBW **(c)** Error in PSLL (dB)

Figure 5.6: Sampling vector resulting in minimum error in HPBW chosen for each number of measurements M

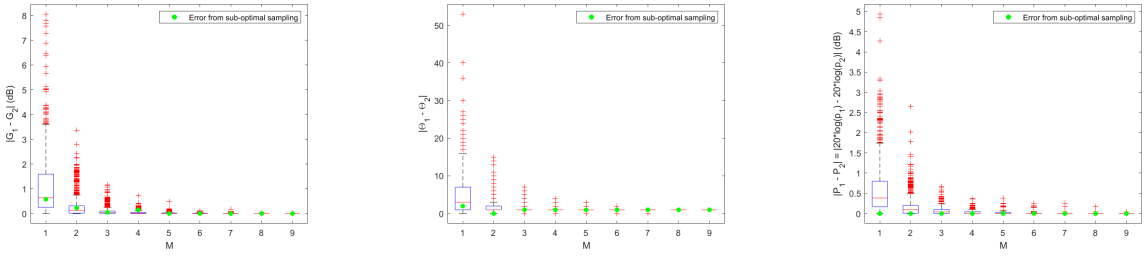

(a) Error in Gain (dB) **(b)** Error in HPBW **(c)** Error in PSLL (dB)

Figure 5.7: Sampling vector resulting in minimum error in PSLL chosen for each number of measurements M

Fig. 5.5 shows the boxplots for error in gain, HPBW and PSLL for the 1000 iterations performed and it also shows the errors over different parameters corresponding to the sampling configuration

that results in the minimum gain. It can be inferred from the figure that the configuration that led to the minimum error in gain does not necessarily give the minimum error in the other quantities as the solution is sub optimal. But if a particular application requires high accuracy in characterization of one of the parameters and can tolerate errors in the other quantities, the corresponding sampling vector can be chosen. This can be done adaptively based on requirements of the system.

A similar analysis (selecting sampling configurations) resulting in minimum error in half power beamwidth and peak side lobe level is done and the results are shown in Fig. 5.6,5.7.

5.3. Conclusions

Customized error metrics pertaining to accuracy in recovery of the gain, half power beamwidth and peak sidelobe level is done in this report and the sampling setup that results in the minimum error in a specific parameter/aspect of the radiation pattern, it is chosen as a sub-optimal sampling vector.

6

Conclusions and recommendations

6.1. Conclusions

The primary objective of the thesis is to find an optimally sparse and adaptive far-field sampling technique and to reconstruct the radiation pattern from an under sampled set measurements. To achieve the same, first the sparsity of the radiation patterns in the transform domain is investigated with DFT and spherical harmonic expansion. A proper comparison of both the sparsifying basis has not been done in literature before. From the comparison, the spherical harmonics provide a much sparser representation for radiation patterns which greatly reduces the number of samples required for reconstruction. For a given accuracy, CS methods using spherical harmonics typically require only 10% of the samples required by the same method using the DFT as sparsity transform.

To find an optimal sampling strategy, the performance of random sample acquisition from regular grid of samples to construct the measurement matrix for the CS problem was investigated. Randomly sampled field measurements from a dense grid of samples is observed to provide near-optimal recovery guarantees for the radiation pattern with high probability for number of measurements M > 2K. A sub-optimal sampling matrix has been arrived at, further improving the minimization in number of samples, from Monte Carlo simulation of upto 1000 runs to choose the sampling scheme with the least error metric.

One of the major novelties in this work is that prior information on the AUT from EM simulations was used to further reduce the number of measurements required to reconstruct the radiation pattern. In this regard, weighted l_1-norm minimization was considered as a better recovery method to reduce the measurements by designing weights using a-priori information on the AUT. From the comparison between basis pursuit and the proposed method, I conclude that the new recovery method provides very significant reduction in the number of samples to be measured while assuring a level of accuracy as decided for the considered requirement. In certain cases, the weighted l_1 minimization required only 65% of the samples as required by recovery using l_1 minimization. Hence the new method offers a 35% reduction in the number of samples as opposed to the benchmark

To further understand the performance of radiation pattern measurement technique and the recovery method, various global and local error metrics were investigated and computed for varying number of measurements. This led to better understanding of the significance of each error quantity to aspects of the radiation pattern, such as the gain, HPBW, PSLL etc.

In order to ensure that the proposed method works when the pattern of the AUT varies with time (due to beam steering, beam forming etc.) or the pattern os distorted due to measurement errors, non-

idealities are introduced to radiation patterns using simulations and the proposed method was able to recover the pattern with non idealities from information on the ideal pattern.

6.2. Recommendations for future work

In the work done in this thesis, the major focus was given to the usage of weighted l_1 minimization for the sparse recovery of the signal. The sampling techniques used are the existing near optimal random selection of samples from a dense equi angular grid of points. However, in order to optimize the overall measurement process, thereby reducing the measurement time, it could be possible to take into account the mechanical constraints and considerations while designing a sensing matrix which has low mutual coherence with the sparsifying basis matrix, or in other words the resulting CS matrix must have low value of mutual coherence with its columns.

One possible direction that was explored during this work was an attempt to optimize the sampling vector using prior information on the AUT.

$$\min \|\underline{x}_{\sim} \otimes PSF - \underline{x}_{\text{sim}}\|_2 \text{ s.t. } \begin{cases} \sum_{t=1} b_{\Omega}(t) = M \\ \underline{b}_{\Omega}(i) \in Z^M \end{cases} \tag{6.1}$$

where x_{sim} is the coefficients obtained from simulations, PSF is the point spread function and b is the sampling vector. Let M be the number of measurements. The reason to formulate this problem is from the fact that if the measurements satisfy maximal incoherence, then the Gram matrix **G** = **I** [39]. This idea of using incoherence measures has also further been explored in the context of MRI in [32].

References

[1] Constantine A Balanis. *ANTENNA THEORY ANALYSIS AND DESIGN THIRD EDITION*. ISBN: 9786468600.

[2] C Beckman and B Lindmark. *The Evolution of Base Station Antennas for Mobile Communications*. Tech. rep.

[3] *IEEE Recommended Practice for Antenna Measurements*. 2021.

[4] Laurent Le Coq et al. "Some contributions for antenna 3d far field characterization at terahertz". In: *Sensors* 21.4 (Feb. 2021), pp. 1–11. ISSN: 14248220. DOI: 10.3390/s21041438.

[5] MD Foegelle. "Antenna Pattern measurement: concepts and techniques". In: *Compliance Engineering* 19.3 (2002), pp. 22–33.

[6] Michael.L Don and Gonzalo.R. Arce. "Antenna Radiation Pattern Compressive Sensing". In: *IEEE Military Communications Conference (MILCOM)*. Los Angeles, CA, USA: IEEE, 2018, pp. 174–181. DOI: 10.1109.

[7] E. de Lera Acedo et al. "SKA aperture array verification system: electromagnetic modeling and beam pattern measurements using a micro UAV". In: *Experimental Astronomy* 45.1 (Mar. 2018), pp. 1–20. ISSN: 15729508. DOI: 10.1007/s10686-017-9566-x.

[8] Giuseppe Virone et al. "Antenna pattern verification system based on a micro unmanned aerial vehicle (UAV)". In: *IEEE Antennas and Wireless Propagation Letters* 13 (2014), pp. 169–172. ISSN: 15361225. DOI: 10.1109/LAWP.2014.2298250.

[9] Giuseppe Virone et al. "UAV-based radiation pattern verification for a small low-frequency array". In: *IEEE Antennas and Propagation Society, AP-S International Symposium (Digest)*. Institute of Electrical and Electronics Engineers Inc., Sept. 2014, pp. 995–996. ISBN: 9781479935406. DOI: 10.1109/APS.2014.6904825.

[10] E. de Lera Acedo et al. "SKALA, a log-periodic array antenna for the SKA-low instrument: design, simulations, tests and system considerations". In: *Experimental Astronomy* 39.3 (Oct. 2015), pp. 567–594. ISSN: 15729508. DOI: 10.1007/s10686-015-9439-0.

[11] S Mirzaei and A Gholipour. "AUT Journal of Electrical Engineering Unmanned Aerial Vehicle Field Sampling and Antenna Pattern Reconstruction Using Bayesian Compressed Sensing". In: 51.1 (2019), pp. 93–100. DOI: 10.22060/eej.2018.14934.5248.

[12] A J van den Biggelaar. *Over-the-air characterization of millimeter-wave integrated antenna systems*. Tech. rep. URL: www.tue.nl/taverne.

[13] Marco Donald Migliore. "Array diagnosis from far-field data using the theory of random partial fourier matrices". In: *IEEE Antennas and Wireless Propagation Letters* 12 (2013), pp. 745–748. ISSN: 15361225. DOI: 10.1109/LAWP.2013.2270931.

[14] Mohammed E. Eltayeb, Tareq Y. Al-Naffouri, and Robert W. Heath. "Compressive Sensing for Millimeter Wave Antenna Array Diagnosis". In: *IEEE Transactions on Communications* 66.6 (June 2018), pp. 2708–2721. ISSN: 00906778. DOI: 10.1109/TCOMM.2018.2790403.

[15] David L. Donoho. “Compressed sensing”. In: *IEEE Transactions on Information Theory* 52.4 (Apr. 2006), pp. 1289–1306. ISSN: 00189448. DOI: 10.1109/TIT.2006.871582.

[16] Simon Foucart and Holger Rauhut. *A Mathematical Introduction to Compressed Sensing*. Springer, 2013. ISBN: 978-0-8176-4948-7. URL: http://www.springer.com/series/4968.

[17] Cosme Culotta-López and Apprimus Verlag. *Fast near-field antenna measurements by application of compressed sensing*. ISBN: 9783863599560.

[18] Arya Bangun, Arash Behboodi, and Rudolf Mathar. “Sensing Matrix Design and Sparse Recovery on the Sphere and the Rotation Group”. In: *IEEE Transactions on Signal Processing* 68 (2020), pp. 1439–1454. ISSN: 19410476. DOI: 10.1109/TSP.2020.2973545.

[19] Arya Bangun and Cosme Culotta-Lopez. “Optimizing Sensing Matrices for Spherical Near-Field Antenna Measurements”. In: *IEEE Transactions on Antennas and Propagation* 71.2 (Feb. 2023), pp. 1716–1724. ISSN: 15582221. DOI: 10.1109/TAP.2022.3227010.

[20] *IEEE Recommended Practice for Near-Field Antenna Measurements Sponsored by the Antenna Standards Committee IEEE Antennas and Propagation Society*. Tech. rep. 2012. DOI: 10.1109/IEEESTD.2012.6375745.

[21] S Farhad Razavi and Yahya Rahmat-Samii. *A New Look at Phaseless Planar Near-Field Measurements: Limitations, Simulations, Measurements, and a Hybrid Solution*. Tech. rep.

[22] Berenice Verdin and Patrick Debroux. *2D and 3D Far-Field Radiation Patterns Reconstruction Based on Compressive Sensing*. Tech. rep. 2016, pp. 47–56.

[23] Emmanuel J. Candes and Michael B. Wakin. “An introduction to compressive sampling: A sensing/sampling paradigm that goes against the common knowledge in data acquisition”. In: *IEEE Signal Processing Magazine* 25.2 (2008), pp. 21–30. ISSN: 10535888. DOI: 10.1109/MSP.2007.914731.

[24] Marco Donald Migliore. “A simple introduction to compressed sensing/sparse recovery with applications in antenna measurements”. In: *IEEE Antennas and Propagation Magazine* 56.2 (Apr. 2014), pp. 14–26. ISSN: 10459243. DOI: 10.1109/MAP.2014.6837061.

[25] Andrea Massa, Paolo Rocca, and Giacomo Oliveri. *Compressive sensing in electromagnetics - A review*. Feb. 2015. DOI: 10.1109/MAP.2015.2397092.

[26] Liang Zhang et al. *Fast Antenna Far-Field Measurement for Sparse Sampling Technology*. Tech. rep. 2018, pp. 145–152.

[27] Berenice Verdin and Patrick Debroux. “Reconstruction of missing sections of radiation patterns using compressive sensing”. In: *IEEE Antennas and Propagation Society, AP-S International Symposium (Digest)*. Vol. 2015-October. Institute of Electrical and Electronics Engineers Inc., Oct. 2015, pp. 780–781. ISBN: 9781479978151. DOI: 10.1109/APS.2015.7304777.

[28] Patrick Debroux and Berenice Verdin. *Compressive Sensing Reconstruction of Wideband Antenna Radiation Characteristics*. Tech. rep. 2017, pp. 1–8.

[29] Benjamin Fuchs et al. “Fast Antenna Far-Field Characterization via Sparse Spherical Harmonic Expansion”. In: *IEEE Transactions on Antennas and Propagation* 65.10 (Oct. 2017), pp. 5503–5510. ISSN: 0018926X. DOI: 10.1109/TAP.2017.2738059.

[30] Bernd Hofmann, Ole Neitz, and Thomas F. Eibert. “On the Minimum Number of Samples for Sparse Recovery in Spherical Antenna Near-Field Measurements”. In: *IEEE Transactions on Antennas and Propagation* 67.12 (Dec. 2019), pp. 7597–7610. ISSN: 15582221. DOI: 10.1109/TAP.2019.2935102.

[31] Benjamin Fuchs et al. *Compressive Sensing Approach for Fast Antenna Far Field Characterization*. Tech. rep. 2018.

[32] Michael Lustig, David Donoho, and John M. Pauly. “Sparse MRI: The application of compressed sensing for rapid MR imaging”. In: *Magnetic Resonance in Medicine* 58.6 (Dec. 2007), pp. 1182–1195. ISSN: 07403194. DOI: 10.1002/mrm.21391.

[33] Felix Krahmer, Christian Kruschel, and Michael Sandbichler. “Total Variation Minimization in Compressed Sensing”. In: (Apr. 2017). URL: http://arxiv.org/abs/1704.02105.

[34] Baozhu Li et al. “Reliable Field Strength Prediction through an Adaptive Total-Variation CS Technique”. In: *IEEE Antennas and Wireless Propagation Letters* 19.9 (Sept. 2020), pp. 1566–1570. ISSN: 15485757. DOI: 10.1109/LAWP.2020.3010410.

[35] Baozhu Li et al. *Total-Variation Compressive Sensing Based on Hybrid Sequential Experimental Design for Field Reconstruction; Total-Variation Compressive Sensing Based on Hybrid Sequential Experimental Design for Field Reconstruction*. Tech. rep. 2019.

[36] Karel Crombecq et al. “A novel hybrid sequential design strategy for global surrogate modeling of computer experiments”. In: *SIAM Journal on Scientific Computing* 33.4 (2011), pp. 1948–1974. ISSN: 10648275. DOI: 10.1137/090761811.

[37] F.A. Musters. *Real-Time 3D Characterization of Antenna Systems*. Tech. rep. 2019. URL: http://repository.tudelft.nl/..

[38] Hamed Masoumi et al. “Structured Sensing Matrix Design for In-sector Compressed mmWave Channel Estimation”. In: *IEEE Workshop on Signal Processing Advances in Wireless Communications, SPAWC*. Vol. 2022-July. Institute of Electrical and Electronics Engineers Inc., 2022. ISBN: 9781665494557. DOI: 10.1109/SPAWC51304.2022.9833949.

[39] Vahid Abolghasemi et al. *ON OPTIMIZATION OF THE MEASUREMENT MATRIX FOR COMPRESSIVE SENSING*. Tech. rep. 2010.

[40] Emmanuel J. Candès, Michael B. Wakin, and Stephen P. Boyd. “Enhancing sparsity by reweighted ℓ1 minimization”. In: *Journal of Fourier Analysis and Applications* 14.5-6 (Dec. 2008), pp. 877–905. ISSN: 10695869. DOI: 10.1007/s00041-008-9045-x.

[41] Rick Chartrand and Wotao Yin. *ITERATIVELY REWEIGHTED ALGORITHMS FOR COMPRESSIVE SENSING*. Tech. rep.

[42] Ivan Lau and Jonathan Jedwab. “Construction of binary matrices for near-optimal compressed sensing”. In: *IEEE International Symposium on Information Theory - Proceedings*. Vol. 2021-July. Institute of Electrical and Electronics Engineers Inc., July 2021, pp. 1612–1617. ISBN: 9781538682098. DOI: 10.1109/ISIT45174.2021.9518096.

[43] Arya Bangun, Arash Behboodi, and Rudolf Mathar. “Coherence Bounds for Sensing Matrices in Spherical Harmonics Expansion”. In: *ICASSP, IEEE International Conference on Acoustics, Speech and Signal Processing - Proceedings*. Vol. 2018-April. Institute of Electrical and Electronics Engineers Inc., Sept. 2018, pp. 4634–4638. ISBN: 9781538646588. DOI: 10.1109/ICASSP.2018.8461805.

[44] Benjamin Fuchs, Laurent Le Coq, and Marco Donald Migliore. “Fast Antenna Array Diagnosis from a Small Number of Far-Field Measurements”. In: *IEEE Transactions on Antennas and Propagation* 64.6 (June 2016), pp. 2227–2235. ISSN: 0018926X. DOI: 10.1109/TAP.2016.2547023.

[45] Sergey Pivnenko et al. “Comparison of antenna measurement facilities with the DTU-ESA 12 GHz validation standard antenna within the EU antenna centre of excellence”. In: *IEEE Transactions on Antennas and Propagation* 57.7 (2009), pp. 1863–1878. ISSN: 0018926X. DOI: 10.1109/TAP.2009.2021934.

[46] Seunghoon Lee and Ho Jin Song. “Accurate Statistical Model of Radiation Patterns in Analog Beamforming including Random Error, Quantization Error, and Mutual Coupling”. In: *IEEE Transactions on Antennas and Propagation* 69.7 (July 2021), pp. 3886–3898. ISSN: 15582221. DOI: 10.1109/TAP.2020.3048528.